Thermodynamics of a Potts-like model for a reconstructed zigzag edge in graphene nanoribbons

J. N. B. Rodrigues[1], P. A. D. Gonçalves[1,2], Jaime E. Santos[2,3,4] and A. H. Castro Neto[5,6]
[1] *Centro de Física do Porto and Departamento de Física, Faculdade de Ciências, Universidade do Porto, Rua do Campo Alegre 687, 4169-007 Porto, Portugal;* [2] *Centro de Física and Departamento de Física, Universidade do Minho, P-4710-057 Braga, Portugal;* [3] *Max Planck Institute for the Physics of Complex Systems, Nöthnitzer Str. 38, D-01187 Dresden, Germany;* [4] *Max Planck Institute for Chemical Physics of Solids, Noethnitzer Str. 40 D-01187 Dresden Germany;* [5] *Graphene Research Centre and Physics Department, National University of Singapore, 2 Science Drive 3, Singapore 117542;* [6] *Department of Physics, Boston University, 590 Commonwealth Avenue Boston MA 02215 USA**
(Dated: September 3, 2013)

We construct a three-color Potts-like model for the graphene zigzag edge reconstructed with Stone-Wales carbon rings, in order to study its thermal equilibrium properties. We consider two cases which have different ground-states: the edge with non-passivated dangling carbon bonds and the edge fully passivated with hydrogen. We study the concentration of defects perturbing the ground-state configuration as a function of the temperature. The defect concentration is found to be exponentially dependent on the effective parameters that describe the model at all temperatures. Moreover, we analytically compute the domain size distribution of the defective domains and conclude that it does not have fat-tails. In an appendix, we show how the exchange parameters of the model can be estimated using DFT results. Such equilibrium mechanisms place a lower bound on the concentration of defects in zigzag edges, since the formation of such defects is due to non-equilibrium kinetic mechanisms.

PACS numbers: 65.80.Ck, 72.80.Vp, 05.50.+q

I. INTRODUCTION

The mechanical exfoliation of graphene,[1] a one-atom thick sheet of carbon atoms arranged in a honeycomb structure, followed by subsequent experiments,[2–4] has given rise to a profusion of studies, both experimental and theoretical (see[5–9] for a list of references) regarding the physical properties of this remarkable material. Such an interest has not subsided to the present date, quite on the contrary.

A simple nearest-neighbor tight-binding approximation of the electronic Hamiltonian in graphene reveals that the honeycomb lattice structure leads to a dispersion relation that is linear around two specific points of the Brillouin zone, the Dirac points. Since the Fermi level of pristine graphene lies at these points, its quasiparticles behave, in a continuum approximation, as massless relativistic fermions with a speed of light equal to the Fermi-velocity ($v_F \approx 10^6 ms^{-1}$).[5,10]

Typically, graphene exhibits high crystal quality, large transparency, being highly conductive and very strong yet flexible.[5,6] All these characteristics place graphene as a good candidate to be used in a variety of technological applications, such as in solar cell technology,[11] in liquid crystal devices,[12] in single molecule sensors,[13] in the fabrication of nano-sized prototype transistors,[14] among many others. Understanding the transport properties of graphene is thus an essential research program towards its application to future nanoscopic devices.

Several of these sought nanoscopic devices will certainly be based on the use of graphene ribbons and graphene quantum dots. In particular, graphene ribbons are usually classified as zigzag or armchair, depending on their edge configuration (see Fig. 1). It is already well established that the electronic properties of these nanostructures are strongly affected by their edge configuration. A nearest-neighbor tight-binding approach leads to the conclusion that zigzag ribbons are metallic regardless of their width, while armchair ribbons can be either semiconducting or metallic, depending on their width. In addition, zigzag ribbons present edge localized states around the Fermi energy.[15–17] However, *ab-initio* calculations predict that graphene ribbons are always semiconducting.[18] Experimental results show that the ribbons' energy gaps increase with decreasing ribbon width.[19]

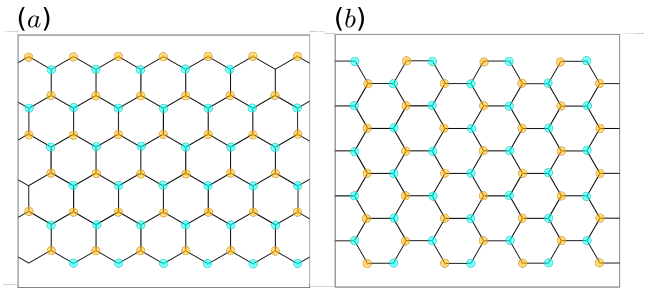

FIG. 1: (Color online) (a) Scheme of zigzag ribbon. (b) Scheme of an armchair ribbon.

It has been shown[20,21] that edge disorder modifies substantially the electronic properties of nanostruc-

tures based on graphene and is responsible for most of the transport properties in these systems. The wavefunctions associated with zigzag edges and vacancies[22] decay very slowly with the distance from the edge because of the absence of a gap in the graphene spectrum. This slow decay leads to strong quantum interference effects that are responsible for destructive quantum interference, Anderson localization, and Coulomb blockade effects in the electrical conductance of graphene-based devices.[23] While most of edge disorder in graphene nanostructures is produced by the method of cutting graphene by hot plasma,[24–26] it also shows conspicuously in chemically driven methods which can be classified as quasi-equilibrium.[27] It thus follows that equilibrium mechanisms, such as the ones described in this work, only place a lower bound on the amount of disorder that can exist in these nanostructures and hence an upper limit in the value of the conductance that can be obtained in these devices.

It is thus of extreme importance for graphene electronics development to understand the effect of edge disorder in the transport properties of graphene ribbons and quantum dots.

One example of disorder appearing at graphene edges are sets of five and seven sided rings of carbon atoms, commonly named in the literature as Stone-Wales (SW) defects.[28] We emphasize that, for the sake of clarity, from now on, we are going to name these structures as *Stone-Wales carbon rings*, limiting the use of the word *defects* to the context of (thermal) disorder.

The SW carbon rings have been observed and found to be meta-stable in the bulk of graphene sheets.[29] Moreover, and regarding graphene's high temperature behavior, it was found that the formation of Stone-Wales carbon rings is the first step in the process of graphene's melting ($T_{melting} \approx 4900$K).[30] Besides, it has been shown through *ab-initio* calculations that whenever SW carbon rings are present in non-passivated graphene nanoribbons, the ribbons energy decreases as the carbon ring approaches the edge of the ribbon.[31] In addition, further *ab-initio* calculations have also shown that the formation of SW carbon rings at the edges of both armchair and zigzag nanoribbons, stabilize them, both energetically and mechanically.[32–34] In particular, in the absence of hydrogen passivation, the zigzag edge is only a meta-stable state, the state where the edge is fully reconstructed with SW carbon rings being the ground-state of the system.[33] Moreover, such total reconstruction of the zigzag edge gives rise to the appearance of a new kind of edge state.[35,36] However, if the zigzag edges are hydrogen passivated, it is the perfect zigzag edge that has the lower energy. The reconstruction of the zigzag edge by SW carbon rings acts as a mechanism that self-passivates the edge.[32] Density functional theory and molecular dynamics calculations corroborate these results, pointing to an energy barrier associated with the edge reconstruction of about 0.4-0.9eV per edge unit cell.[32,37–39]

These types of zigzag edge reconstructions (see Fig. 2), are claimed to be stable only at very low hydrogen pressure (well below ambient conditions) and very low temperatures.[40] However, reconstructions of the zigzag (as well as armchair) edges have been recently observed with high-resolution TEM,[41–43] albeit under rather extreme conditions, namely, the graphene flake is bombarded with high-energy electrons (80 keV) that remove C atoms from the sheet. The recent work of Suenaga *et al.*,[44] on single-atom spectroscopy using low-voltage STEM, provides a *non-destructive* method of identifying the edge configuration of graphene ribbons, as does the work of Warner *et al.* on the observation of real-time dynamics of dislocations using high-resolution TEM.[45] Moreover, refinements in other techniques, such as Raman spectra of the edges,[46] STM images of the edges,[32] or coherent electron focusing[47] may help in identifying edge reconstructions.

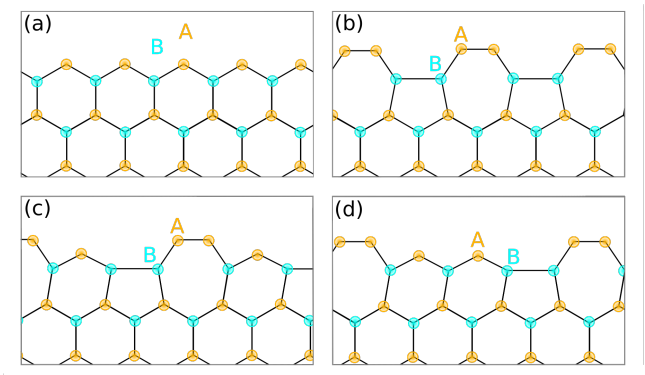

FIG. 2: (Color online) (a) Scheme of clean zigzag edge, usually named zz. (b) Scheme of a totally reconstructed (with SW carbon rings) zigzag ribbon, usually named $zz(57)$. In (c) and (d), we present schemes of a partially reconstructed zigzag ribbon, respectively, $zz(576)$ and $zz(5766)$.

In this work, we construct a one-dimensional three-color (or three-state) Potts-like model so as to describe the reconstruction of the zigzag edge with SW carbon rings, due to thermal fluctuations. From such a model, we will extract thermodynamic properties of the zigzag edge, both in the absence and in the presence of hydrogen passivation. These properties include the number of pentagons and heptagons at an edge, the concentration of domains formed by pentagon-heptagon pairs within larger groups of hexagons or the concentration of domains formed by hexagons within larger groups of pentagon-heptagon pairs (depending on the state of passivation of the edge), and the size-distribution of both kinds of minority domains at the edge. These quantities are then used to characterize the degree of disorder of the zigzag edge due to thermal fluctuations.

The simple model presented in this work indicates that if the nanoribbon edge behaves as a one-dimensional system with short-range interactions, it will present a finite concentration of defects at any finite temperature. Moreover, the average length of such defects is finite at any

non-zero temperature. This is in sharp contrast with the case of the one-dimensional ferromagnetic Ising model, where domains of minority spins, which can be viewed as the defects perturbing the ground-state configuration, have an average length that diverges at infinitesimally small temperatures, destroying the ferromagnetic order. We believe that such distinct behavior is due to the lack of a full $\mathbf{Z}_3$ symmetry in the three-color Potts-like model. Furthermore, we are able to compute analytically the distribution of lengths of defective domains (DSD), as well as the concentration of such domains. We show that the DSD has no fat-tails.

From an experimental point of view, the concentration of defective domains is the most relevant quantity that one can compute, since it is found to be exponentially dependent on the values of the effective exchange parameters of the model. Hence, the measurement of the concentration of defects would allow for a sensitive determination of these parameters. Since such measurements have not yet been performed, we have estimated these parameters using DFT calculations. Depending on the actual value of the effective parameters, the concentration of defects can become quite large at room temperatures, and may thus have a significant effect on the conductivity of the zigzag ribbon.

The structure of this paper is as follows: Section II will be devoted to the presentation of the three-color Potts-like model that describes the thermodynamics of the edge with SW carbon rings and of the results extracted from it. We will first present a descriptive outline of the model. In sub-Section II A, we will compute the thermodynamic quantities characterizing the edge, using a transfer matrix formulation of the Potts-like model and we will analyze their dependence both on the temperature and on the exchange parameters. Finally, in Section III, we will present our conclusions. We leave to the appendices the computation of the exchange parameters from *ab-initio* results (Appendix A), the calculation of correlation functions in the three-color Potts-like model, using the transfer matrix formalism (Appendix B), and the explicit computation of the size-distribution of domains of polarized and unpolarized spins (Appendix C).

II. POTTS-LIKE MODEL OF THE ZIGZAG EDGE

We will study graphene zigzag edges with SW carbon rings, employing a one-dimensional three-color Potts-like model, where each color is assigned to a different polygon of the edge (hexagons, heptagons and pentagons). We label each edge unit cell, i. e. each polygon at the edge, by the integer variable $i = 0, 1, \cdots, 2N$, with the state of such a cell being described by the ternary variable $\sigma_i = 0, +1, -1$, according to whether the polygon forming that cell in the reconstructed edge is an hexagon, heptagon or pentagon. We consider a nearest-neighbor coupling between adjacent cells only (the validity of this assumption will be justified in Appendix A), which leaves us with 9 possible values for the couplings $J_{\sigma_i\sigma_{i+1}}$, depending on the neighboring states. We take as reference state with zero energy the perfect zigzag edge, thus $J_{00} = 0$. Taking into account the experimental observations, we will exclude from the model states where two pentagons or heptagons sit at neighboring sites, i.e. pairings of heptagons or pentagons are forbidden and one has $J_{++} = J_{--} = \infty$. Invariance under inversion implies that the order in a pentagon-heptagon, pentagon-hexagon or heptagon-hexagon pair is irrelevant, and thus $J_{-+} = J_{+-}$, $J_{0+} = J_{+0}$ and $J_{0-} = J_{-0}$. Moreover, since heptagons and pentagons are created in pairs through the transference of C atoms between neighboring sites, we will assume that the probability of creation of a pentagon or an heptagon is the same, which implies that $J_{0-} = J_{0+}$. Hence, the 9 initial possible values of the couplings are reduced to two free parameters: $J_{0+} = \gamma > 0$, which reflects the fact that the formation of defects costs energy and $J_{+-} = \delta$, which may be negative or positive depending on whether the totally reconstructed edge has lower or higher energy than the pristine zigzag edge (i.e., depending on the state of passivation of the edges, as discussed above). Finally, since C atoms are conserved, one should, strictly speaking, consider a model with as many heptagons as pentagons, i.e. one should work in a subspace of the state-space having the overall magnetization $M = \sum_{i=0}^{2N} \sigma_i = 0$. Such a constraint can be written in terms of an imaginary applied magnetic field over which one has to integrate, once the eigenvalues of the transfer matrix of the Potts-like model have been computed. In such a case, the eigenvalues can no longer be simply determined. We will therefore relax this constraint and we will only implement it on average, as $\langle M \rangle = 0$ in 1d. Note, moreover, that although some of the edge observation techniques[41–43] are highly energetic and cause the ejection of C atoms from the edges, the system cannot be considered to be in thermodynamic equilibrium when such ejection occurs and the model introduced below is therefore not applicable.[41] It may however be applicable after a characteristic relaxation time, such that the thermodynamics of the edge would be described in terms of an effective temperature, dependent on the energy deposited by the electron beam and the heat conduction process in graphene. One would expect the number of (remaining) C atoms in the edge to be conserved in this late-time regime. In Fig. 3, we present a cartoon of three possible configurations of the edges and how they translate into configurations of the three-color Potts-like model.

A. Edge thermodynamics

In the previous paragraphs, we have shown how to map the different configurations of a reconstructed edge of a graphene zigzag ribbon to those of a three-color nearest-neighbor Potts-like model. We now wish to use such a

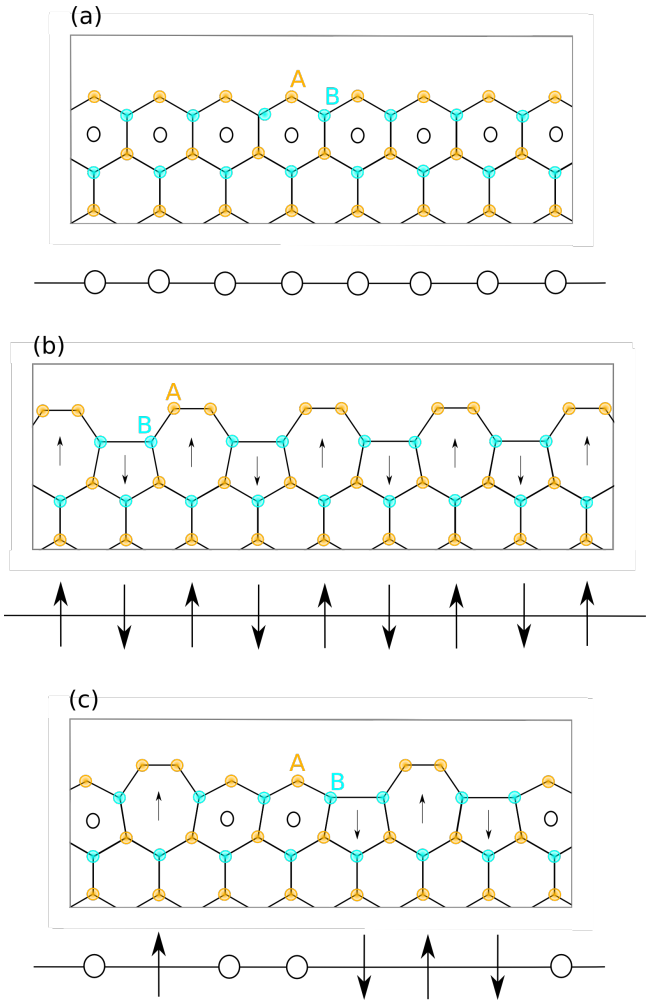

FIG. 3: (Color online) Scheme of the Potts-like model (three-color) for the zigzag edge with SW carbon rings. In (a), a clean zigzag edge, zz, is shown. In (b), a zigzag edge which is totally reconstructed with SW carbon rings, $zz(57)$, is presented. In (c), a zigzag edge with an arbitrary reconstruction is shown.

model to compute useful quantities relating to the thermodynamics of the edges. As is usual in one-dimensional models with nearest neighbor interactions, the speediest way to compute thermodynamic properties, including spin-spin correlation functions, is to express these quantities in terms of a transfer matrix.[48] In the case of the model presented above, the transfer matrix reads:

$$\mathbf{T} = \begin{pmatrix} 0 & e^{-\beta\gamma} & e^{-\beta\delta} \\ e^{-\beta\gamma} & 1 & e^{-\beta\gamma} \\ e^{-\beta\delta} & e^{-\beta\gamma} & 0 \end{pmatrix} \quad , \tag{1}$$

where $\beta = 1/k_B T$ and γ and δ are the parameters introduced above and computed in Appendix A. The model, as defined by Eq. (1), represents a limiting case of the Blume-Emery-Griffiths model in one dimension.[49–51] One eigenvalue of the transfer matrix, $\lambda_0 = -e^{-\beta\delta}$, can be readily identified, after which the other two are also easily

Configuration	$\sum_i' \sigma_i^2$	$\sum_i' \delta_{\sigma_i \sigma_{i+1},-1}$	Difference
$0+0$	1	0	1
$0-0$	1	0	1
$0+-0$	2	1	1
$0-+0$	2	1	1
$0+-+0$	3	2	1
$0-+-0$	3	2	1

TABLE I: Contribution of a $+-$ domain for the different observables.

computed from the quadratic equation that is obtained from the application of, e.g., Ruffini's rule to the cubic secular equation. These two eigenvalues are given by $\lambda_\pm = \frac{1}{2}\left[1 + e^{-\beta\delta} \pm \sqrt{(1-e^{-\beta\delta})^2 + 8\,e^{-2\beta\gamma}}\right]$. At all temperatures above zero, λ_+ is the largest eigenvalue. At $T = 0$ and if $\delta > 0$, this is also the case, however if $\delta \leq 0$ the largest eigenvalue may be doubly or thrice degenerate, which reflects the degeneracy of the ground-state of the system (see Appendix B).

The free energy of the system is given by $F = -k_B T \ln(\mathrm{Tr}\,\mathbf{T}^{2N})$ from which we have that in the thermodynamic limit $N \to \infty$ the free energy per site is simply proportional to the logarithm of the largest eigenvalue, i.e.

$$f = -k_B T \ln\left\{\frac{1}{2}\left[1 + e^{-\beta\delta} + \sqrt{(1-e^{-\beta\delta})^2 + 8\,e^{-2\beta\gamma}}\right]\right\} . \tag{2}$$

We are primarily interested in the disorder caused either to a clean zigzag edge (ground-state of the passivated edge) or to a totally reconstructed zigzag edge (ground-state of the non-passivated edge) through the effect of temperature, which leads these configurations [as depicted in Fig. 3(a) and (b)] to evolve into 3(c). For a totally passivated edge, a measure of such disorder can be obtained by counting the number of domains of polarized spins (heptagons and pentagons) that exist between sites with 0-spin (hexagons), the converse being valid for the non-passivated edge. As an example, in Fig. 3(c) one has two domains of polarized spins. In order to be able to count them, consider the contribution of a domain, both to $\sum_i \sigma_i^2$, which measures the number of heptagons or pentagons in the system, and to $\sum_i \delta_{\sigma_i\sigma_{i+1},-1}$, which measures the number of heptagon-pentagon links (see Table I). Since each domain contributes exactly 1 to the difference between these two quantities, one sees that the number of domains is given by the difference of these two operators. Note however, that whenever the spin chain has no 0-spins, the difference between these two operators gives 0. As a consequence, the correct expression for the average domain concentration of $\pm$-spin

domains, $\langle n_{d\pm}\rangle = \langle N_{d\pm}\rangle/2N$, is given by

$$\langle n_{d\pm}\rangle = \frac{1}{2N}\left[\sum_i \left(\langle\,\sigma_i^2\,\rangle - \langle\,\delta_{\sigma_i\sigma_{i+1},-1}\,\rangle\right) + \left\langle \prod_i \sigma_i^2 \right\rangle\right]. \tag{3}$$

If one uses periodic boundary conditions (PBCs) and the spin chain is not uniformly polarized (either all the sites with spin 0, or all the sites with alternating polarized spins $+-+-+-$), the number of domains of $\pm$-spins is always equal to the number of domains of 0-spins. In such a case, we have $N_{d\pm} = N_{d0} \equiv N_d$. As a consequence, we can express $\langle n_{d0}\rangle$ in terms of $\langle n_{d\pm}\rangle$, just by considering the following sum over all spin configurations,

$$\langle n_{d0}\rangle \;=\; \langle n_{d\pm}\rangle - \frac{1}{2N}\left[\left\langle \prod_i \sigma_i^2 \right\rangle - \left\langle \prod_i (1-\sigma_i^2) \right\rangle\right] \tag{4}$$

Note that in the thermodynamic limit, $2N \to \infty$, the thermal averages of the products can be neglected, resulting in $\langle n_{d0}\rangle \approx \langle n_{d\pm}\rangle$.

One can separately compute the correlation functions $\langle\,\sigma_i^2\,\rangle$ and $\langle\,\delta_{\sigma_i\sigma_{i+1},-1}\,\rangle$, as is done in Appendix B. However, it is simpler to consider instead generating fields in the partition sum that are coupled to $\sum_i \sigma_i^2$ and to $\sum_i \delta_{\sigma_i\sigma_{i+1},-1}$. One then concludes, using the transfer matrix formalism, that the concentration of polarized sites, $\langle n_{pol}\rangle = \frac{\langle N_{pol}\rangle}{2N} = \frac{1}{2N}\sum_i \langle\,\sigma_i^2\,\rangle$, is given, in the thermodynamic limit, by

$$\langle n_{pol}\rangle = \frac{1}{2}\frac{\partial f}{\partial \gamma} + \frac{\partial f}{\partial \delta}\,. \tag{5}$$

The concentration of unpolarized sites is simply obtained from $\langle n_{unp}\rangle = 1 - \langle n_{pol}\rangle$. Moreover, the concentration of links between polarized sites, defined as, $\langle n_{+-}\rangle = \frac{\langle N_{+-}\rangle}{2N} = \frac{1}{2N}\sum_i \langle\,\delta_{\sigma_i\sigma_{i+1},-1}\,\rangle$, is given, in the thermodynamic limit, by

$$\langle n_{+-}\rangle = \frac{\partial f}{\partial \delta}\,. \tag{6}$$

Similarly, the concentration of links between unpolarized sites, is simply obtained from $\langle n_{00}\rangle = 1 - \langle n_{+-}\rangle - \langle n_{\pm 0}\rangle$, where $n_{\pm 0}$ stands for the concentration of links between polarized and unpolarized sites. Note that in the thermodynamic limit, $\langle n_{\pm 0}\rangle \approx 2\langle n_{d0}\rangle \approx 2\langle n_{d\pm}\rangle$.

If one substitutes in equation (3) the expression for $\langle n_{pol}\rangle$ and for $\langle n_{+-}\rangle$, as given by Eq. (5) and Eq. (6), one can write for $\langle n_{d\pm}\rangle$, in the thermodynamic limit, the result

$$\langle n_{d\pm}\rangle = \frac{1}{2}\frac{\partial f}{\partial \gamma}\,. \tag{7}$$

Substituting Eq. (2) in Eq. (5), we obtain for $\langle n_{pol}\rangle$

$$\langle n_{pol}\rangle \;=\; \frac{4e^{-2\beta\gamma} + e^{-\beta\delta}(-1+e^{-\beta\delta}+\theta)}{(1+e^{-\beta\delta}+\theta)\theta}, \tag{8}$$

where $\theta = \sqrt{(1-e^{-\beta\delta})^2 + 8e^{-2\beta\gamma}}$. A plot of this quantity as a function of T/γ, for selected values of the ratio δ/γ, is shown in Fig. 4.

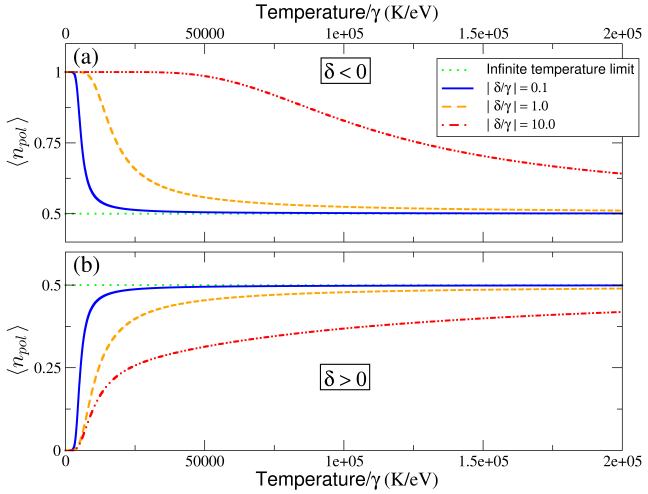

FIG. 4: (Color online) Plot of the concentration of polarized spins, $\langle n_{pol}\rangle$, either for a non-passivated edge (a) and for a hydrogen-passivated one (b) as a function of T/γ, for three different values of the ratio δ/γ. The full dark blue lines stand for $|\delta/\gamma| = 0.1$; the dashed orange lines stand for $|\delta/\gamma| = 1.$; the dash-dotted red lines stand for $|\delta/\gamma| = 10.$. Note that the δ/γ ratio is negative for the non-passivated case (because $\delta < 0$) and positive for the passivated case (because then $\delta > 0$). The green dotted flat line represents the infinite temperature limit for both cases, which is 1/2. Since we are using PBC, $\langle n_{unp}\rangle = 1 - \langle n_{pol}\rangle$.

Substituting Eq. (2) in Eq. (6), we obtain for $\langle n_{+-}\rangle$

$$\langle n_{+-}\rangle \;=\; \frac{e^{-\beta\delta}(-1+e^{-\beta\delta}+\theta)}{(1+e^{-\beta\delta}+\theta)\theta}\,. \tag{9}$$

A plot of Eq. (9) as a function of T/γ, for selected values of the ratio δ/γ, is shown in Fig. 5.

Finally, substituting Eq. (2) in Eq. (7), we obtain for $\langle n_{d\pm}\rangle$

$$\langle n_{d\pm}\rangle = \frac{4e^{-2\beta\gamma}}{(1+e^{-\beta\delta}+\theta)\theta}, \tag{10}$$

which gives the concentration of domains of polarized spins as a function of the temperature and of the coupling parameters. A plot of $\langle n_{d\pm}\rangle$ as a function of T/γ, is shown for selected values of the ratio δ/γ in Fig. 6.

In both the non-passivated case and the hydrogen-passivated one, the concentration of domains of polarized sites, n_d, is very small at low temperatures (Fig. 6). However, from Figs. 4 and 5, we conclude that these two situations are substantially different. In the former, at low temperature, we have a small number of very large polarized domains, with very few 0-spins between them. In contrast, in the latter case, at low temperature, we have a low number of very small polarized domains, with large domains of 0-spins between them. This is merely a manifestation of the fact that the two cases have different ground-states.

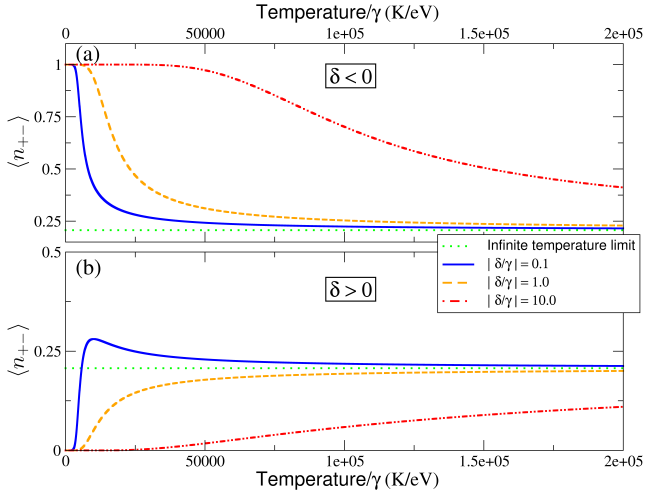

FIG. 5: (Color online) Plot of the concentration of links between polarized spins, $\langle n_{+-}\rangle$, either for a non-passivated edge (a) and for a hydrogen-passivated one (b) as a function of T/γ, for three different values of the ratio δ/γ. The full dark blue lines stand for $|\delta/\gamma| = 0.1$; the dashed orange lines stand for $|\delta/\gamma| = 1.$; the dash-dotted red lines stand for $|\delta/\gamma| = 10.$. Note that the δ/γ ratio is negative for the non-passivated case (because $\delta < 0$) and positive for the passivated case (because then $\delta > 0$). The green dotted flat line represents the infinite temperature limit for both cases, which is $1/(2+2\sqrt{2})$. Since we are using PBC, $\langle n_{00}\rangle = 1 - \langle n_{+-}\rangle - \langle n_{\pm 0}\rangle$.

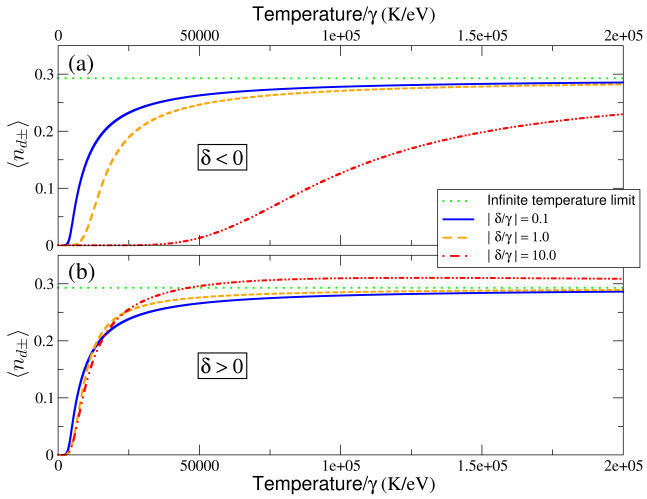

FIG. 6: (Color online) Plot of the concentration of domains of polarized spins, $\langle n_{d\pm}\rangle$, for a non-passivated edge (a) and a hydrogen-passivated one (b) as a function of T/γ, for three different values of the ratio δ/γ. The full dark blue lines stand for $|\delta/\gamma| = 0.1$; the dashed orange lines stand for $|\delta/\gamma| = 1.$; the dash-dotted red lines stand for $|\delta/\gamma| = 10.$. Note that the δ/γ ratio is negative for the non-passivated case (because $\delta < 0$) and positive for the passivated case (because $\delta > 0$ in such a case). The green dotted flat line represents the infinite temperature limit for both cases, which is $1/(2+\sqrt{2})$. Since we are using PBCs, in the thermodynamic limit, $\langle n_{d0}\rangle \approx \langle n_{d\pm}\rangle$.

The DSD of polarized spins, $\mathcal{P}_{\pm}(L) = \langle N^{\pm}_{d_L}/N_{d\pm}\rangle$, where L is the length of the domain and $N^{\pm}_{d_L}$ is the number of $+-$ domains with size equal to L, can be computed exactly using the transfer matrix formalism for the three-states Potts-like model developed above. The detailed (and rather lengthy) calculation is presented in Appendix C. We obtain, in the thermodynamic limit, the result

$$\mathcal{P}_{\pm}(L) \;=\; \frac{\lambda_+ e^{\beta\delta} - 1}{\left(\lambda_+ e^{\beta\delta}\right)^L}\,. \tag{11}$$

Likewise, we have also computed the DSD of unpolarized spins, $\mathcal{P}_0(L) = \langle N^0_{d_L}/N_{d0}\rangle$ (where $N^0_{d_L}$ is the number of 0 domains with size equal to L), see again Appendix C. The result that we have obtained is given, in the thermodynamic limit, by

$$\mathcal{P}_0(L) \;=\; \frac{\lambda_+ - 1}{\lambda_+^L}. \tag{12}$$

In Eqs. (11) and (12), $\lambda_+ = (1 + e^{-\beta\delta} + \theta)/2$. Equations (11) and (12) and their derivation are the main result of this work. One should note that L is geometrically distributed in both cases. In Fig. 7, we plot the DSD as a function of L (with logarithmic scale in the y-axis), for different values of T/γ and of the ratio δ/γ. We plot the DSD of unpolarized spins when the edge is non-passivated [panel (a)] and the DSD of polarized spins when the edge is hydrogen-passivated [panel (b)].

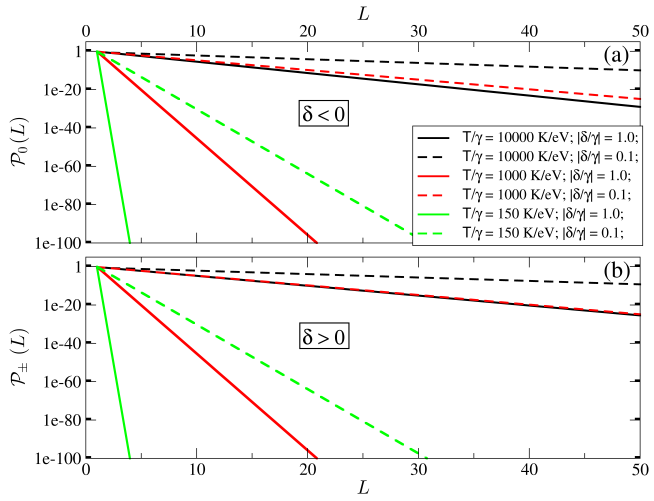

FIG. 7: (Color online) Plot of the DSD, $\mathcal{P}(L)$, for several temperatures and several values of the ratio δ/γ. The DSD is plotted with a logarithmic scale in the y-axis. (a) DSD of unpolarized spins in a non-passivated edge ($\gamma > 0$ and $\delta < 0$). (b) DSD of polarized spins in a hydrogen-passivated edge ($\gamma > 0$ and $\delta > 0$). The black, red, and light green curves stand, respectively, for $T/\gamma = 10000$ K/eV, $T/\gamma = 1000$ K/eV and $T/\gamma = 150$ K/eV. The full and dashed lines, stand, respectively, for $|\delta/\gamma| = 1.0$ and $|\delta/\gamma| = 0.1$.

The characteristic functions of these two distributions can be readily computed from Eqs. (11) and (12). We

obtain in the case of domains with polarized spins,

$$\hat{\mathcal{P}}_{\pm}(w) \;=\; \frac{\lambda_{+}e^{\beta\delta}-1}{\lambda_{+}e^{\beta\delta}e^{-iw}-1}\,, \tag{13}$$

while in the case of unpolarized domains, we have

$$\hat{\mathcal{P}}_{0}(w) \;=\; \frac{\lambda_{+}-1}{\lambda_{+}e^{-iw}-1}\,. \tag{14}$$

Since these distributions are geometric distributions and hence all their moments exist, their characteristic functions, as given by Eqs. (13) and (14), are analytic at $w = 0$, as can be seen by direct inspection. This result is equivalent to the statement that the distributions do not have fat tails.

The first moment of these distributions, gives us the average size of, respectively, the domains of polarized and unpolarized spins. The explicit expression for the average size of the domains of polarized spins reads [see Appendix C, Eq. (C34)],

$$\bar{L}_{\pm} \;=\; \frac{\lambda_{+}e^{\beta\delta}}{\lambda_{+}e^{\beta\delta}-1}\,, \tag{15}$$

while the average size of the domains of unpolarized spins reads

$$\bar{L}_{0} \;=\; \frac{\lambda_{+}}{\lambda_{+}-1}\,. \tag{16}$$

It is interesting to compare the results given in Eqs. (15) and (16) with the results obtained from a different (and rather natural) definition of the average domain size, namely $\tilde{L}_{\pm} \equiv \langle n_{pol}\rangle/\langle n_{d\pm}\rangle$ and $\tilde{L}_{0} \equiv \langle n_{unp}\rangle/\langle n_{d0}\rangle$. We obtain for $\tilde{L}_{\pm}$, the result

$$\tilde{L}_{\pm} \;=\; \frac{4e^{-2\beta\gamma}+e^{-\beta\delta}(-1+e^{-\beta\delta}+\theta)}{4e^{-2\beta\gamma}},\,. \tag{17}$$

Moreover, in the thermodynamic limit, $\tilde{L}_{0}$ can be written in terms of $\tilde{L}_{\pm}$ as $\tilde{L}_{0} = \langle n_{unp}\rangle/\langle n_{d0}\rangle = \big(1 - \langle n_{pol}\rangle\big)/\langle n_{d0}\rangle \approx 1/\langle n_{d0}\rangle - \tilde{L}_{\pm}$. If we now substitute λ_{+} by its definition in equations (15) and (16), we can show that $\bar{L}_{\pm} = \tilde{L}_{\pm}$ and $\bar{L}_{0} = \tilde{L}_{0}$, i.e. the two definitions yield identical results. This equality suggests that the statistical variables N_{d_L}/N_d and N_d are independent in the thermodynamic limit, i.e. that the fraction of domains with size L is independent of the number of the said domains in the limit of an infinite system. However, we were as yet unable to prove that such independence holds in the whole temperature range.

In Fig. 8, we plot the average domain size of the minor domains in each of the two cases ($\bar{L}_{0}$ for non-passivated edges and $\bar{L}_{\pm}$ for hydrogen-passivated edges - see the previous paragraph) as a function of T/δ, for selected values of the ratio δ/γ.

From Figs. 4-8, we confirm that irrespective of the value of the dimensionless temperature T/γ, the system always presents a finite concentration of defects at any finite temperature, as is to be expected for a one-dimensional system with short-range interactions. However, since our model does not possess the full $\mathbf{Z}_3$ symmetry characteristic of a true Potts-like model (in which case the Peierls argument does apply), the results obtained are qualitatively different from those obtained for an Ising chain, where the formation of domains of macroscopic size fully destroys order at any $T \neq 0$ (in our case, the energy of formation of a domain does depend on the domain's size). In contrast with what happens in the one-dimensional Ising model, here the disorder tends to zero with decreasing temperature, being exactly zero only at $T = 0$. Depending on the exchange parameters of the system, the concentration of minority domains at room temperature (and hence the degree of disorder of the edge at such temperature) may or may not present a large value. In addition, the smaller the ratio δ/γ is, the less stable the edge is to the effect of thermal disorder. As expected, the average mean size of the minority domains increases with temperature. Finally, the larger the ratio δ/γ is, the larger is the size of the minority domains. This is to be expected, so as to minimize the number of domain walls (links 0+ and 0-, whose exchange parameter is γ) relatively to the number of +- links (whose exchange parameter is δ).

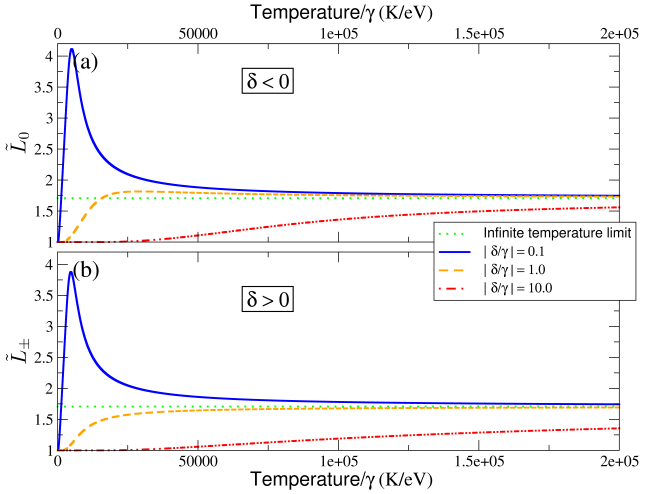

FIG. 8: (Color online) Plot of the average domain size of the minority domains as a function of T/γ. (a) Average domain size of unpolarized domain sites (unpassivated edge), $\tilde{L}_0$. (b) Average domain size of polarized domain sites (hydrogen-passivated edge), $\tilde{L}_{\pm}$. The different curves in each plot, stand for three different values of the ratio δ/γ. The full dark blue lines stand for $|\delta/\gamma| = 0.1$; the dashed orange lines stand for $|\delta/\gamma| = 1.0$; the dash-dotted red lines stand for $|\delta/\gamma| = 10.0$. Note that the δ/γ ratio is negative for the non-passivated case (since $\delta < 0$) and positive for the passivated case (since $\delta > 0$). The green dotted flat line represents the infinite temperature limit for both cases, which is $1 + 1/\sqrt{2}$.

In Appendix A, based on *ab-initio* calculations that we have both performed ourselves (case $\mathcal{C}_1$) and that we have obtained from the existing literature (case $\mathcal{C}_2$), we

compute specific values of the exchange parameters of the model that we have introduced, $(\delta_{\mathcal{C}_1}, \gamma_{\mathcal{C}_1})$ and $(\delta_{\mathcal{C}_2}, \gamma_{\mathcal{C}_2})$. Using these particular values of the exchange parameters, we present there plots of the thermodynamic quantities introduced in Eqs. (8)-(17), as functions of the absolute temperature, rather than presenting them as functions of the reduced temperature T/γ and the ratio δ/γ. From these results, one can conclude that, in both cases $\mathcal{C}_1$ and $\mathcal{C}_2$, the exchange parameters calculated from the *ab-initio* are such that the ground-state edge configuration is robust with respect to the effect of thermal disorder.

Nevertheless, it should also be stated that due to the sensitivity of the system's thermodynamic behavior on the precise numerical value of the exchange parameters (see Appendix A), this conclusion may well be challenged in the future, in case more detailed *ab-initio* calculations yield different numerical values for the exchange parameters. We should emphasize in this regard that the *ab-initio* calculations that we have performed were done using narrow ribbons, where an interaction between the two edges of the ribbon can be observed. Moreover, these calculations did not take into account either the spin-polarization of electrons on the edge, or the relaxation of the atoms along the transverse direction of the ribbon and that such complications need to be addressed in future publications.

Note that our model is necessarily an oversimplified one. Firstly, it assumes that the state of passivation of the edge is a quenched variable determined by the concentration of H_2 molecules present in the atmosphere of the experiment. This is not an entirely realistic assumption, since it is to be expected that the binding-unbinding of H atoms to an hexagon or heptagon (pentagons have no dangling-bonds to which H atoms can bind to) is influenced by temperature and pressure. Taking such observation into account in our model would imply the introduction of a chemical potential regulating the chemical equilibrium between the passivating atoms attached to the edge and those in the atmosphere surrounding the ribbon. Moreover, in the most general case, one would also have to allow the state of passivation of an hexagon or heptagon to be a statistical variable, since the bare exchange parameters between neighboring sites should depend on their state of passivation. This would imply the introduction of a Potts-like model with a higher number of colors (corresponding to both hydrogen-passivated and non-passivated edge polygons).

Finally, it is to be expected that in an experiment, the edge may be passivated by other atomic or molecular species present in the gaseous environment surrounding the ribbon (namely oxygen, nitrogen, water, etc.) and not just by hydrogen. In order to take into account the presence of competing species, one would need to consider a Potts-like model with a yet higher number of colors, together with additional exchange parameters associated with the interaction between different kinds of passivation between neighboring polygons, each of which would need to be computed from *ab-initio* simulations. Moreover, one would have to introduce a chemical potential for each species, regulating the chemical equilibrium between the passivating atoms of that species attached to the edge and those in the atmosphere surrounding the ribbon. This would make the model increasingly difficult to study using a simple analytical approach as the one presented above.

III. CONCLUSION

In this work, we have treated the zigzag edge (in the presence of SW carbon rings) of a graphene ribbon as a one-dimensional system and introduced a three-color Potts-like model to study its thermodynamic properties regarding the presence of thermal disorder. We have shown how to extract the effective parameters that describe the model from *ab-initio* calculations and how to use these numerical values to determine the temperature dependence of the defect size and defect concentration.

As is to be expected for a one-dimensional system with short-range interactions, we concluded that the edge is always disordered at any finite temperature. More importantly, this model allowed us to make quantitative predictions for the concentration and size of the defective domains at a given temperature, both for the totally passivated and for the totally non-passivated zigzag edge. The defect concentration was found to be exponentially dependent on the exchange parameters of the model. Depending on the actual value of these parameters, the concentration of defects can become quite large at room temperatures, and may thus have a significant effect on the conductivity of the zigzag ribbon. We have also computed the DSD for the totally passivated and non-passivated edge and have concluded that these distributions do not have fat-tails.

Edge disorder may strongly influence the conductance of graphene based-devices. However, the equilibrium mechanisms described in this work only place a lower bound on the quantity of disorder present at the edges of graphene nanostructures. Equivalently, they put an upper limit in the value of the conductance that can be obtained in these devices.[20,21]

Acknowledgments

We acknowledge helpful discussions with N. Peres, J. Lopes dos Santos, P. Ribeiro, E. Lage, R. Ribeiro and A. Läuchli. J. N. B. R. was supported by the Portuguese Foundation for Science and Technology (FCT) through Grant No. SFRH/BD/44456/2008. J.E.S. acknowledges support by the Visitors Program of the MPIPkS and by the MPICPfS at the early stages of this work. J.E.S. work contract is financed in the framework of the Program of Recruitment of Post Doctoral Researchers for the Portuguese Scientific and Technological System, within the Operational Program Human Potential (POPH) of

the QREN, participated by the European Social Fund (ESF) and national funds of the Portuguese Ministry of Education and Science (MEC). He also acknowledges support provided to the current research project by FEDER through the COMPETE Program and by FCT in the framework of the Strategic Project PEST-C/FIS/UI607/2011. A. H. C. N. acknowledges DOE grant DE-FG02-08ER46512, ONR grant MURI N00014-09-1-1063, and the NRF-CRP award "Novel 2D materials with tailored properties: beyond graphene" (R-144-000-295-281).

APPENDIX A: THE EXCHANGE PARAMETERS FROM *AB-INITIO* RESULTS

In this appendix we will show how one can compute the exchange parameters of the Potts-like model, from *ab-initio* results of zigzag ribbons with reconstructed edges.

The energy per edge atom of periodic edge configurations such as zz, $zz(57)$, $zz(576)$ and $zz(576^n)$ (where n stands for the number of hexagons in the periodic edge configuration - see Fig. 2), can be computed either using the three-color Potts-like model proposed in the main text (for particular values of the parameters γ and δ), or using the *ab-initio* results for the edge energies computed from density functional theory. From a least squares method, we can then compute the exchange parameters, γ and δ, of the Potts-like model, in such a way that the latter describes, to a good degree of accuracy, the *ab-initio* results.

The edge energies (per unit cell of the perfect zigzag edge) of different periodic reconstructions of the edge, for example, $zz(57)$, $zz(576)$, $zz(5766)$, etc., are given, in the scope of the previously introduced Potts-like model, by

$$E\big(zz(57)\big) = J_{+-}, \tag{A1a}$$

$$E\big(zz(576^n)\big) = \frac{J_{+-}+2J_{+0}+(n-1)J_{00}}{n+2}, \tag{A1b}$$

$$E\big(zz\big) = J_{00}, \tag{A1c}$$

where n stands for the number of edge hexagons present in a unit cell. Expressing these energies relative to the clean edge energy $\Delta E\big(zz(576^n)\big) = E\big(zz(576^n)\big) - E\big(zz\big)$, with the latter set to zero (i.e. $J_{00}=0$, as above), we obtain,

$$\Delta E\big(zz(57);\delta,\gamma\big) = \delta, \tag{A2a}$$

$$\Delta E\big(zz(576^n);\delta,\gamma\big) = \frac{\delta+2\gamma}{n+2}, \tag{A2b}$$

where we made the substitutions $J_{+-}=\delta$ and $J_{+0}=\gamma$.

We now consider the energy ϵ_n of the edge $zz(576^n)$ referred to the pristine zigzag edge, as obtained from *ab-initio* calculations (see Fig. 9). The exchange parameters γ and δ can be obtained from a minimization of the sum of the squared differences between $\Delta E\big(zz(576^n)\big)$, as given by Eqs. (A2), and ϵ_n,

$$S(\delta,\gamma) = \sum_{n=0}\Big[\Delta E\big(zz(576^n);\delta,\gamma\big)-\epsilon_n\Big]^2. \tag{A3}$$

The uncertainty on the computed exchange parameters, is given by

$$\sigma_z = \sum_{n=0}\Big[\sigma_n^2\Big(\frac{\partial z}{\partial \epsilon_n}\Big)^2\Big], \tag{A4}$$

where z stands for γ or δ, whose expression as a function of ϵ_n is computed from minimization of $S(\delta,\gamma)$, and where σ_n are the uncertainties in the *ab-initio* energies ϵ_n.

In order to obtain indicative values for the exchange parameters of the three-color Potts-like model introduced in the text, we have both used *ab-initio* results on non-passivated zigzag edges already published in the literature,[33] and have ourselves performed *ab-initio* calculations on hydrogen-passivated edges. In Fig. 9, we plot the edge energies (relative to the energy of the pristine zigzag edge), obtained from *ab-initio* calculations of edge reconstructed zigzag ribbons with both hydrogen-passivated edges and non-passivated edges.

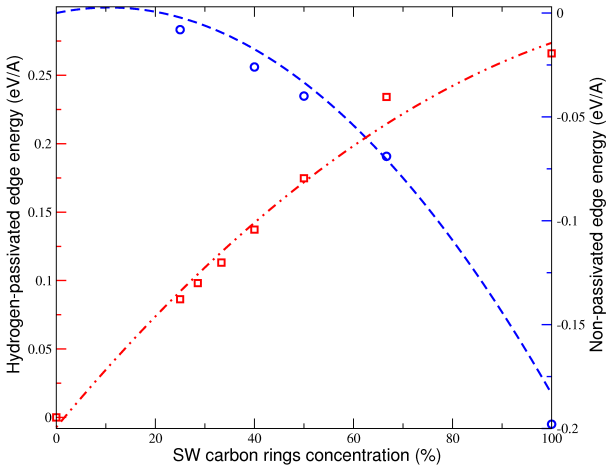

FIG. 9: (Color online) Energies of the partially reconstructed edges, measured relative to the pristine zz edge, as a function of the SW carbon rings concentration. Dots represent the edge energies obtained from *ab-initio* calculations, while dashed lines correspond to a polynomial interpolation of the results obtained from the Potts-like model using the exchange parameters computed with the least squares method. The red squares and red dash-dotted line represent the results obtained for hydrogen-passivated zigzag ribbons (left y-axis), whereas the blue circles and blue dashed line represent the edge energies of non-passivated zigzag ribbons (right y-axis).

From the *ab-initio* results summarized in Fig. 9, and after employing the method just described to compute the exchange parameters in both cases, we obtain the following values for the exchange parameters:

- Hydrogen-passivated edge (case $\mathcal{C}_1$): We have performed *ab-initio* calculations for hydrogen-passivated ribbons with various concentrations of SW carbon rings (see Fig. 9).[1] We have assumed the same value $\sigma_n = 0.01\,eV$ for all uncertainties.[2] The values obtained for the parameters were $\gamma_{\mathcal{C}_1} = (0.53 \pm 0.03)\,eV$ and $\delta_{\mathcal{C}_1} = (0.65 \pm 0.04)\,eV$.

- Non-passivated edge (case $\mathcal{C}_2$): The *ab-initio* results used in this case were extracted from the work of Huang *et al.*.[33] We have assumed the same value $\sigma_n = 0.01\,eV$ for all uncertainties.[3] The values obtained for the parameters were $\gamma_{\mathcal{C}_2} = (0.03 \pm 0.02)\,eV$ and $\delta_{\mathcal{C}_2} = (-0.49 \pm 0.03)\,eV$.

In Fig. 9, we plot the results obtained from *ab-initio* calculations (isolated dots), compared with the polynomial interpolation of these results (dashed-lines), which was obtained from the least squares method, as described above. The fact that these curves are in good agreement with the *ab-initio* results justifies *a posteriori* the use of a Potts-like model with only nearest-neighbor interactions.

Using the above values for the exchange parameters, the concentration of polarized spins, $\langle n_{pol}\rangle$, defined in Eq. (5), the concentration of links between polarized spins, $\langle n_{+-}\rangle$, defined in Eq. (6), the concentration of polarized domains, $\langle n_{d\pm}\rangle$, defined in Eq. (7) and the average domain size of the minor domains, L_{Av}, defined in Eq. (17), acquire the form presented in Fig. 10.

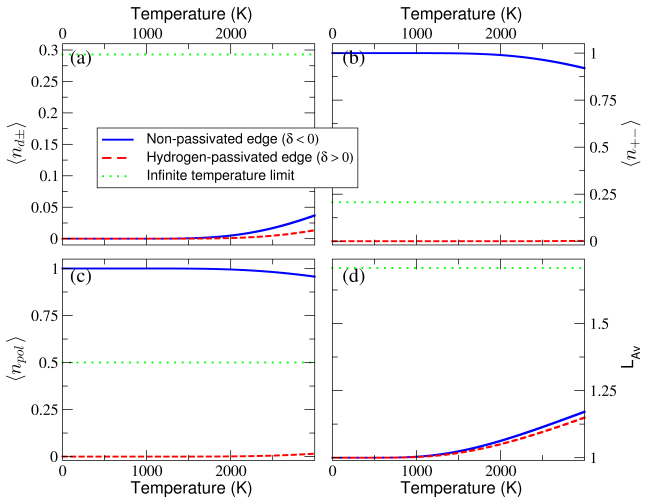

FIG. 10: (Color online) Plot of the four thermodynamic quantities introduced in the main text, for the values of the exchange parameters obtained from the ab-initio results: $\delta_{\mathcal{C}_1} = 0.66$ and $\gamma_{\mathcal{C}_1} = 0.52$ for the hydrogen-passivated edge (red dashed curves); $\delta_{\mathcal{C}_2} = -0.49$ and $\gamma_{\mathcal{C}_2} = 0.03$ for the non-passivated edge (blue full curves). Panel (a) shows the concentration of polarized domains, $\langle n_{d\pm}\rangle$. Panel (b) shows the concentration of links between polarized spins, $\langle n_{+-}\rangle$. Panel (c) shows the concentration of polarized spins, $\langle n_{pol}\rangle$. Panel (d) shows the average minor domain size, L_{Av}. The dotted green flat lines represent the infinite temperature limit of each quantity.

Using the exchange parameters calculated above, one concludes that the concentration of polarized domains in the non-passivated case at room temperature has a value $\langle n_d\rangle \simeq 6.65\times10^{-18}$ defects per unit cell of pristine zigzag edge (or $\langle n_d\rangle \simeq 5.41\times10^{-8}$ defects per meter).[4] In addition, at room temperature, the unpolarized domains have an average domain size of $\bar{L}_0^{MF} \simeq 1$ unit cells (or $\bar{L}_0^{MF} \simeq 1.23\times10^{-10}m$). These small unpolarized domains are on average $1.85\times10^{7}m$ apart from each other.

In the case of a hydrogen-passivated edge, the above calculated parameters give, at room temperature, a concentration of polarized domains of $\langle n_d\rangle \simeq 1.50\times10^{-22}$ per unit cell of pristine zigzag edge (or $\langle n_d\rangle \simeq 1.22\times10^{-14}$ defects per meter). The polarized domains have a mean size of $\bar{L}_{\pm}^{MF} \simeq 1$ unit cells (or $\bar{L}_{\pm}^{MF} \simeq 1.23\times10^{-10}m$). The small domains of polarized spins are on average $8.20\times10^{13}m$ apart from each other.

These results show that, with the given set of effective parameters as computed from the *ab-initio* methods, the ground-states in both the non-passivated case (totally reconstructed edge) and the hydrogen-passivated case (pristine zigzag edge) are very stable with respect to the effect of thermal disorder.

---

[1] The Density Functional Theory (DFT) calculations were performed using the code AIMPRO,[52] under the Local Density Approximation (LDA). The Brillouin-zone (BZ) was sampled for integrations according to the scheme proposed by Monkhorst-Pack.[53] The core states were accounted for by using the dual-space separable pseudo-potentials by Hartwigsen, Goedecker, and Hutter.[54] The valence states were expanded over a set of *s*-, *p*-, and *d*-like Cartesian-Gaussian Bloch atom-centered functions. The total energies in the self-consistency cycle were converged such that changes in energy between two iterations and the electrostatic energy associated with the difference between input and output charge densities were both less than 2.7×10^{-4} eV. The k-point sampling ranged from $12\times4\times1$ for the $zz(57)$ edge to $4\times4\times1$ for the $zz(57666666)$ edge and the atoms were relaxed in order to find their equilibrium positions. The ribbons were simulated within a supercell geometry using vacuum layers of $12.7\mathring{A}$ in the ribbon plane and $10.6\mathring{A}$ in the normal direction in order to avoid interactions between ribbons in adjacent cells.

[2] We have estimated the uncertainty associated with our *ab-initio* calculations of the edge energy per angstrom (for every SW carbon ring periodicity at the edges), to be given by $\sigma' \approx 0.01eV$ per unit cell of pristine edge.

[3] From Figure 5(*a*) of Huang et al.,[33] we have estimated the uncertainty associated with the edge energies per unit of length to be $\sigma' = 0.004eV/\mathring{A}$. As in this work we are using units of energy per unit cell of the pristine edge, $\sigma = \sigma' \times 1.42\sqrt{3} \approx 0.01eV$.

[4] Note that, in the thermodynamic limit, the number of polarized domains is equal to the number of unpolarized domains, and consequently, the corresponding domain densities are also equal.

However, we should note that in our model, the sensitivity of the thermodynamic quantities on the values of the exchange parameters is large. In order to illustrate such fact, consider for instance that the exchange parameters were reduced to 1/4 of the values which we determined above. This would imply that the room temperature concentration of defects would be increased by several orders of magnitude: in the non-passivated case, it would be increased to $\langle n_d \rangle \simeq 7.01 \times 10^5$ defects per meter (the average distance between neighboring defects would be $1.43 \mu m$); in the hydrogen-passivated case, the defect concentration would be increased to $\langle n_d \rangle \simeq 4.82 \times 10^4$ defects per meter (the average distance between neighboring defects would be $20.8 \mu m$ apart). Consequently, if more detailed *ab-initio* calculations were to give significantly smaller exchange parameters, this would imply that the edge ground-state would be much less robust to the effect of thermal disorder.

APPENDIX B: CORRELATION FUNCTIONS OF THE POTTS-LIKE MODEL

The computation of correlation functions of a one-dimensional Potts-model in a periodic system involves the computation of the trace of a string of operators.[50] For instance, the magnetization of the system can be written, using the cyclic invariance of the trace, as

$$\begin{aligned} \langle \sigma_i \rangle &= \frac{1}{Z_{2N}} \sum_{\{\sigma\}} \mathbf{T}_{\sigma_1\sigma_2} \dots \mathbf{T}_{\sigma_{i-1}\sigma_i} \, \sigma_i \, \mathbf{T}_{\sigma_i\sigma_{i+1}} \dots \mathbf{T}_{\sigma_{2N}\sigma_1} \\ &= \frac{1}{Z_{2N}} \mathrm{Tr}(\hat{\sigma} \, \mathbf{T}^{2N}) \,, \end{aligned} \tag{B1}$$

where $\mathbf{T}_{\alpha\beta}$ are the individual matrix elements of the transfer matrix in Eq. (1), while $Z_{2N} = \mathrm{Tr}(\mathbf{T}^{2N}) = \lambda_+^{2N} + \lambda_0^{2N} + \lambda_-^{2N}$ is the partition function of the model and $\hat{\sigma}$ is the 3×3 matrix

$$\hat{\sigma} = \begin{pmatrix} 1 & 0 & 0 \\ 0 & 0 & 0 \\ 0 & 0 & -1 \end{pmatrix} \quad . \tag{B2}$$

Eq. (B1) shows that the magnetization is space-independent. Since the trace in Eq. (B1) is independent of the basis used for its calculation, we choose the one that diagonalizes $\mathbf{T}$,

$$| \, \lambda_0 \, \rangle = \frac{1}{\sqrt{2}} \begin{pmatrix} 1 \\ 0 \\ -1 \end{pmatrix} \quad , \tag{B3}$$

which is the eigenvector corresponding to the eigenvalue $\lambda_0 = -e^{-\beta\delta}$ and

$$| \, \lambda_\pm \, \rangle = \begin{pmatrix} \alpha_\pm \\ \beta_\pm \\ \alpha_\pm \end{pmatrix} \quad , \tag{B4}$$

which are the eigenvectors corresponding to the eigenvalues $\lambda_\pm = \frac{1}{2} \left[1 + e^{-\beta\delta} \pm \sqrt{(1 - e^{-\beta\delta})^2 + 8 \, e^{-2\beta\gamma}} \right]$, where $\alpha_\pm$ is given by

$$\alpha_\pm = \frac{\lambda_\pm - 1}{\sqrt{2} \, [(\lambda_\pm - 1)^2 + 2 \, e^{-2\beta\gamma})]^{1/2}} \,, \tag{B5}$$

and where $\beta_\pm^2 = 1 - 2\alpha_\pm^2$ (normalization condition). It can be easily checked that these three vectors form an orthonormal basis. Expressing the trace in terms of this basis, one obtains for the magnetization Eq. (B1), the result

$$\langle \sigma_i \rangle = \frac{1}{Z_{2N}} \sum_{\mu=0,\pm1} \lambda_\mu^{2N} \, \langle \, \lambda_\mu \, | \, \hat{\sigma} \, | \, \lambda_\mu \, \rangle = 0 \,, \tag{B6}$$

since $\langle \, \lambda_\mu \, | \, \hat{\sigma} \, | \, \lambda_\mu \, \rangle = 0$ for each one of the eigenvectors of $\mathbf{T}$. This equality merely reflects the symmetry of the model with respect to an interchange of $+$ with $-$ spins that is present by construction. In order to infer the existence of a phase transition at $T = 0$ in the absence of a (infinitesimal) field that explicitly breaks this symmetry, one needs to consider the behavior of higher-order correlation functions.

The spin-spin correlation function $\langle \, \sigma_i \sigma_{i+j} \, \rangle$ is given by

$$\begin{aligned} \langle \, \sigma_i \sigma_{i+j} \, \rangle &= \frac{1}{Z_{2N}} \mathrm{Tr}(\mathbf{T}^{2N-j} \hat{\sigma} \, \mathbf{T}^j \hat{\sigma}) \\ &= \frac{1}{Z_{2N}} \sum_{\mu,\nu} \lambda_\mu^{2N-j} \lambda_\nu^j \, | \, \langle \, \lambda_\mu \, | \, \hat{\sigma} \, | \, \lambda_\nu \, \rangle \, |^2 , \end{aligned} \tag{B7}$$

where we have used a representation of the unit-operator in terms of the eigenstates of $\mathbf{T}$, on going from the first to the second line of Eq. (B7). At $T \neq 0$ and in the thermodynamic limit $N \to \infty$, the only term in the numerator of Eq. (B7) that survives, is the one with $\nu = 0$, $\mu = +1$ and $Z_{2N} \approx \lambda_+^{2N}$. Thus, we obtain in this case, since $\langle \, \lambda_+ \, | \, \hat{\sigma} \, | \, \lambda_0 \, \rangle = \sqrt{2} \alpha_+$,

$$\langle \, \sigma_i \sigma_{i+j} \, \rangle = 2\alpha_+^2 \, \left(\frac{\lambda_0}{\lambda_+} \right)^j \,. \tag{B8}$$

If $T \neq 0$, $\langle \, \sigma_i \sigma_{i+j} \, \rangle \to 0$ if $j \to \infty$, showing that the magnetization of the system is zero at any finite temperature, as is to be expected for any system with $\mathbb{Z}_2$ symmetry in 1d. At $T = 0$, one has to distinguish three cases: $\delta > 0$, in which case $\lambda_+ \to 1$ and both λ_0 and λ_- go to zero. In that case, Eq. (B7) still holds and the ground-state is simply the $0000 \dots$ state, with no associated magnetization. If, on the other hand $\delta < 0$, $\lambda_+ \to \infty$, $\lambda_0 \to -\infty$ and $\lambda_- \to 0$. In that case, one has to consider again Eq. (B6), since the terms $\langle \, \lambda_+ \, | \, \hat{\sigma} \, | \, \lambda_0 \, \rangle$ and $\langle \, \lambda_0 \, | \, \hat{\sigma} \, | \, \lambda_+ \, \rangle$ contribute equally to it. Thus, we obtain $\langle \, \sigma_i \sigma_{i+j} \, \rangle = (-1)^j$, which shows that the anti-ferromagnetic states '$\dots + - + - \dots$' and '$\dots - + - + \dots$ are the two degenerate ground-states. In this case, the system shows a transition to a finite (staggered) magnetization at zero temperature. Finally,

if $\delta = 0$, $\lambda_\pm \to 1$, $\lambda_0 \to -1$ and all terms $\langle\, \lambda_\pm \,|\, \hat{\sigma} \,|\, \lambda_0 \,\rangle$ and $\langle\, \lambda_0 \,|\, \hat{\sigma} \,|\, \lambda_\pm \,\rangle$ contribute to Eq. (B7). We obtain $\langle\, \sigma_i \sigma_{i+j} \,\rangle = \frac{2}{3}\,(-1)^j$, which shows that there are three degenerate ground-states '$\ldots 0000 \ldots$', '$\ldots + - + - \ldots$' and '$\ldots - + - + \ldots$'. One can also show that a phase transition is present when $\delta \leq 0$, if one writes equation Eq. (B8) as $\langle\, \sigma_i \sigma_{i+j} \,\rangle = 2\alpha_+^2\,(-1)^j\, e^{-j/\xi}$, where $\xi = 1/\ln(\lambda_+/\mid \lambda_0 \mid)$ is the correlation length of the model. If $\delta > 0$, $\xi = 0$ at $T = 0$ and no phase transition occurs, but if $\delta \leq 0$, $\xi \to \infty$ at $T = 0$ indicating the presence of a phase transition. Note that the presence of a phase transition has at most a marginal effect on the results presented in the main text, since such a phase transition is due to the existence of a $\mathbb{Z}_2$ symmetry in the model, whereas the formation of minority domains of either 0's or $+-$ relies on states not related by such a symmetry.

One can also use the transfer matrix formalism to compute the probability $\langle\, \delta_{\sigma_i \sigma_{i+j},-1} \,\rangle$ that the spins at sites i and $i+j$ are anti-parallel. One uses the identity $\delta_{\sigma_i \sigma_{i+j},-1} = \frac{1}{2}\,\sigma_i \sigma_{i+j}(\sigma_i \sigma_{i+j} - 1)$, which can be easily checked by substituting σ_i and σ_{i+j} by their values $0, \pm 1$. Since we have already computed the spin-spin correlation function above, we are left with the computation of $\langle\, \sigma_i^2 \sigma_{i+j}^2 \,\rangle$. Following the same steps as above, we obtain

$$\langle\, \sigma_i^2 \sigma_{i+j}^2 \,\rangle = \frac{1}{Z_{2N}} \sum_{\mu,\nu} \lambda_\mu^{2N-j} \lambda_\nu^j \mid \langle\, \lambda_\mu \,|\, \hat{\sigma}^2 \,|\, \lambda_\nu \,\rangle \mid^2, \quad \text{(B9)}$$

where $\hat{\sigma}^2$ is the matrix

$$\hat{\sigma}^2 = \begin{pmatrix} 1 & 0 & 0 \\ 0 & 0 & 0 \\ 0 & 0 & 1 \end{pmatrix} \quad . \quad \text{(B10)}$$

At $T \neq 0$, the only terms that need to be considered in Eq. (B9) are those involving $\langle\, \lambda_+ \,|\, \hat{\sigma}^2 \,|\, \lambda_+ \,\rangle$ and $\langle\, \lambda_+ \,|\, \hat{\sigma}^2 \,|\, \lambda_0 \,\rangle$. Taking this into account, as well as the expression Eq. (B8) for $\langle\, \sigma_i \sigma_{i+j} \,\rangle$, one finally obtains for $\langle\, \delta_{\sigma_i \sigma_{i+j},-1} \,\rangle$, the result

$$\begin{aligned} \langle\, \delta_{\sigma_i \sigma_{i+j},-1} \,\rangle \;&=\; 2\alpha_+^4 + 2\alpha_+^2 \alpha_-^2 \left(\frac{\lambda_0}{\lambda_+}\right)^j \\ &\quad - \alpha_+^2 \left(\frac{\lambda_0}{\lambda_+}\right)^j . \end{aligned} \quad \text{(B11)}$$

Using Eq. (B8) with $j = 0$ and Eq. (B11) with $j = 1$ in the expression for $n_d = \langle\, \sigma_i^2 \,\rangle - \langle\, \delta_{\sigma_i \sigma_{i+1},-1} \,\rangle$ given in section II A, we obtain $n_d = 2\alpha_+^2(1 - e^{-\beta\delta}/\lambda_+)$, which is exactly the result given in Eq. (10).

APPENDIX C: THE DOMAIN SIZE DISTRIBUTION

In what follows, we will compute the DSD of the 0-spins domains and of $\pm$-spin domains. Throughout the computation, we will assume PBCs for the system. We will illustrate the computation of the DSD of 0-spins, pinpointing the differences with the computation of the DSD of $\pm$-spins.

In the context of the exact calculation of the DSD, the thermal average of the distribution of the sizes of domains of 0-spins is defined by

$$\bar{L}_0 \;=\; \sum_{L=1}^{2N} L\, P_0(L), \quad \text{(C1)}$$

where $P_0(L)$ is the domain size distribution of domains of 0-spins (thermal average of the fraction of domains of size L). This quantity is given by

$$P_0(L) \;=\; \left\langle \frac{N_{d_L}^0}{N_{d0}} \right\rangle, \quad \text{(C2)}$$

where $N_{d_L}^0$ stands for the number of domains of 0-spins with size L, while N_{d0} stands for the total number of 0-spins domains regardless of their size. An analogous expression can be written for the DSD of $\pm$-spins.

We start by defining the operator that verifies in every possible way if the spin i is in a domain of spins 0 with size L,

$$f_{i,L}^0 \;\equiv\; \sum_{k=0}^{L-1} \left[\sigma_{i-k-1}^2 \Big(\prod_{\gamma=0}^{L-1} \big(1 - \sigma_{i-k+\gamma}^2\big) \Big) \sigma_{i-k+L}^2 \right]. \quad \text{(C3)}$$

The above definition is valid for cases where the domain has a size $L \leq 2N-2$, where $2N$ stands for the total number of spins in the one-dimensional chain. In the case where $L = 2N-1$ and $L = 2N$, this definition is modified. It reads

$$f_{i,L=2N-1}^0 \;\equiv\; \sum_{k=0}^{2N-2} \left[\sigma_{i-k-1}^2 \prod_{\gamma=0}^{2N-2} \big(1 - \sigma_{i-k+\gamma}^2\big) \right], \quad \text{(C4)}$$

$$f_{i,L=2N}^0 \;\equiv\; \prod_{\gamma=0}^{2N-1} \big(1 - \sigma_{i+\gamma}^2\big). \quad \text{(C5)}$$

We can analogously define an operator verifying in every possible way if the spin i is in a domain of spins $\pm$ with size L, namely $f_{i,L}^\pm$. To do this, it suffices to substitute, in Eqs. (C3)-(C5), the operators σ^2 by $1 - \sigma^2$. For $L \leq 2N-2$, $f_{i,L}^\pm$ reads

$$f_{i,L}^\pm \;\equiv\; \sum_{k=0}^{L-1} \left[\big(1 - \sigma_{i-k-1}^2\big) \prod_{\gamma=0}^{L-1} \sigma_{i-k+\gamma}^2 \big(1 - \sigma_{i-k+L}^2\big) \right], \quad \text{(C6)}$$

whereas, for $L = 2N-1$ and $L = 2N$, we have

$$f_{i,L=2N-1}^\pm \;\equiv\; \sum_{k=0}^{2N-2} \left[\big(1 - \sigma_{i-k-1}^2\big) \prod_{\gamma=0}^{2N-2} \sigma_{i-k+\gamma}^2 \right], \quad \text{(C7)}$$

$$f_{i,L=2N}^\pm \;\equiv\; \prod_{\gamma=0}^{2N-1} \sigma_{i+\gamma}^2. \quad \text{(C8)}$$

Given this, if for a given configuration of the edge, we want to count the number of unpolarized spins in domains of size L, N_L^0, we just need to perform the sum of the operators $f_{i,L}^0$ over every site in the one-dimensional chain. Explicitly, it reads

$$N_L^0 \equiv \sum_{i=1}^{2N} f_{i,L}^0. \tag{C9}$$

From such a quantity, we can easily extract the number of 0-spin domains with size L of a particular configuration. We have thus that the number of domains of 0-spins with size L is given by

$$N_{d_L}^0 \equiv \frac{N_L^0}{L} = \sum_{i=1}^{2N} \frac{f_{i,L}^0}{L}. \tag{C10}$$

In addition, if we want to count all the domains of 0-spins, irrespective of their size, we just have to sum $N_{d_L}^0$ over all possible sizes L,

$$N_{d0} \equiv \sum_{L=1}^{2N} N_{d_L}^0 = \sum_{L=1}^{2N}\sum_{i=1}^{2N} \frac{f_{i,L}^0}{L}. \tag{C11}$$

Instead of defining the operator counting the total number of domains of 0-spins as was done in Eq. (C11), we can use an equivalent and simpler expression for such an operator. It reads

$$N_{d0} \equiv \begin{cases} \frac{N_{\pm 0}}{2} & \text{if } L \neq 2N, \\ 1 & \text{if } L = 2N, \end{cases} \tag{C12}$$

where $N_{\pm 0}$ stands for the number of links between polarized and unpolarized spins, while the term $\delta_{L_0,2N}$ accounts for the situation in which all the spins in the chain are unpolarized, in which case there are no links between polarized and unpolarized spins, but there is one domain of 0-spins occupying the entire chain. This operator can be written explicitly as

$$\begin{aligned} N_{d0} \equiv & \frac{1}{2}\sum_{i=1}^{2N}\left[\sigma_i^2(1-\sigma_{i+1}^2) + (1-\sigma_i^2)\sigma_{i+1}^2\right] \\ & + \prod_{i=1}^{2N}(1-\sigma_i^2). \end{aligned} \tag{C13}$$

Such a definition is introduced because the operator $N_{\pm 0}/2$ is not equivalent to the operator counting the number of domains in a one-dimensional spin chain. This operator, in fact, counts the number of links between polarized and unpolarized spins ($+0$, -0, $0+$ and $0-$) divided by two. Whenever the spin configuration is such that there are links between polarized and unpolarized spins, this operator is equivalent to the operator giving the number of domains. However, when there are no links between polarized and unpolarized spins, this operator always yields 0, not being able to distinguish between the cases where all the spins are polarized (and thus the number of unpolarized spin domains is $N_{d0} = 0$) and the case where all the spins are unpolarized (and thus the number of unpolarized spin domains is $N_{d0} = 1$). In order to account for these cases, the term $\prod_{i=1}^{2N}(1-\sigma_i^2)$ is added to the definition of N_{d0}, giving 1 when the whole spin chain is unpolarized.

We can write analogous equations to Eqs. (C9)-(C13) for the case of polarized spins. The operator counting the number of polarized spins in domains of $\pm$-spins, $N_L^{\pm}$, reads

$$N_L^{\pm} \equiv \sum_{i=1}^{2N} f_{i,L}^{\pm}, \tag{C14}$$

while the operator counting the number of domains (of $\pm$-spins) with size L, reads

$$N_{d_L}^{\pm} \equiv \frac{N_L^{\pm}}{L} = \sum_{i=1}^{2N} \frac{f_{i,L}^{\pm}}{L}. \tag{C15}$$

The total number of $\pm$-spins domains, irrespectively of their size, $N_{d\pm}$, reads

$$N_{d\pm} \equiv \sum_{L=1}^{2N} N_{d_L}^{\pm} = \sum_{L=1}^{2N}\sum_{i=1}^{2N} \frac{f_{i,L}^{\pm}}{L}, \tag{C16}$$

which, in analogy with what was done for N_{d0}, can be rewritten, reading

$$N_{d\pm} \equiv \frac{1}{2}\sum_{i=1}^{2N}\left[\sigma_i^2 + \sigma_{i+1}^2 - \sigma_i^2\sigma_{i+1}^2 + \sigma_i\sigma_{i+1}\right] + \prod_{i=1}^{2N}\sigma_i^2. \tag{C17}$$

Note that the term $\prod_{i=1}^{2N}\sigma_i^2$, evaluates to 1 when all the spins are polarized (forming a polarized spin domain with a length $L = 2N$) and to 0 in all other cases.

We can now obtain the DSD of 0-spins by computing the thermal average of the ratio $N_{d_L}^0/N_{d0}$ [see Eq. (C2)]. The computation of thermal averages of ratios can be performed using the following mathematical trick

$$\begin{aligned} \left\langle \frac{N_{d_L}^0}{N_{d0}} \right\rangle &= \left\langle \int_0^\infty N_{d_L}^0 e^{-uN_{d0}} \mathrm{d}u \right\rangle \\ &= \int_0^\infty \left\langle N_{d_L}^0 e^{-uN_{d0}} \right\rangle \mathrm{d}u, \end{aligned} \tag{C18}$$

where in the last equality we assumed that we can interchange the integration and averaging procedures, regardless of the size of the system.

In the above thermal average, given by the sum over all configurations, we need to exclude the two configurations with all spins polarized, since $N_{d_L}^0 = 0$ and $N_{d0} = 0$ in such case, yielding indeterminate terms to the sum. This is equivalent to the computation of the conditioned probability of having a domain of unpolarized spins with a particular size L, given that there are

domains of 0-spins in the one-dimensional chain. Excluding these terms changes the partition function, Z_{2N}, from $Z_{2N}=\lambda_+^{2N}+\lambda_0^{2N}+\lambda_-^{2N}$ to $Z'_{2N}=Z_{2N}-2e^{-2N\beta\delta}=\lambda_+^{2N}-\lambda_0^{2N}+\lambda_-^{2N}$. In addition, note that the sums over all the configurations must also exclude the terms associated with this configuration.

We can thus rewrite Eq. (C18) as

$$\left\langle \frac{N^0_{d_L}}{N_{d0}} \right\rangle = \int_0^\infty \sum_{\{\sigma\}'} \frac{N^0_{d_L} e^{-\beta E(\{\sigma\})-uN_{d0}}}{Z'_{2N}} \mathrm{d}u, \quad \text{(C19)}$$

where $\{\sigma\}'$ indicates that the sum is performed over all the configurations except the two configurations with all spins polarized. Note, however that in Eq. (C19), summing over $\{\sigma\}'$ or over all the configurations, $\{\sigma\}$, yields the same result, because the two configurations with all spins polarized contribute with $N^0_{d_L}=0$ to the sum.

The version of Eq. (C19) for domains of polarized spins is obtained by substituting in Eq. (C19) $N^0_{d_L}$ and N_{d0} by respectively, $N^\pm_{d_L}$ and $N_{d\pm}$, while $Z'_{2N}=Z_{2N}-1=\lambda_+^{2N}+\lambda_0^{2N}+\lambda_-^{2N}-1$, since in this case the configuration yielding $N_{d\pm}=0$ is that with all the spins unpolarized. Explicitly, it reads

$$\left\langle \frac{N^\pm_{d_L}}{N_{d\pm}} \right\rangle = \int_0^\infty \sum_{\{\sigma\}'} \frac{N^\pm_{d_L} e^{-\beta E(\{\sigma\})-uN_{d\pm}}}{Z'_{2N}} \mathrm{d}u, \quad \text{(C20)}$$

a. The exact expression of the DSD

In order to obtain the exact expression of the DSD of 0-spins, we need to compute the integrand of Eq. (C19). The sum over all configurations in Eq. (C19) can still be performed using the transfer matrix formalism (see Appendix B). However, here we have to use a modified transfer matrix, which absorbs the exponential of the number of domains N_{d0} appearing in Eq. (C19) in the definition given by Eq. (1). It reads

$$\widetilde{T} = \begin{pmatrix} 0 & e^{-\beta\widetilde{\gamma}} & e^{-\beta\delta} \\ e^{-\beta\widetilde{\gamma}} & 1 & e^{-\beta\widetilde{\gamma}} \\ e^{-\beta\delta} & e^{-\beta\widetilde{\gamma}} & 0 \end{pmatrix}, \quad \text{(C21)}$$

where we have rescaled the exchange parameter γ to $\widetilde{\gamma}=\gamma+u/(2\beta)$. Both the eigenvalues, $\widetilde{\lambda}_+$, $\widetilde{\lambda}_0$, $\widetilde{\lambda}_-$ and the eigenvectors, $|\widetilde{\lambda}_0\rangle$, $|\widetilde{\lambda}_0\rangle$, $|\widetilde{\lambda}_0\rangle$, of this $\widetilde{T}$-matrix, have exactly the same form of those obtained for the T-matrix, with γ substituted by $\widetilde{\gamma}$. However, both the eigenvalues and the eigenvectors now depend on the integration variable u, through the rescaled exchange parameter $\widetilde{\gamma}$.

As mentioned above, this new $\widetilde{T}$-matrix originates from the definition of N_{d0} [see Eq. (C13)]. Note however, that there is a subtlety in the definition of the $\widetilde{T}$-matrix in Eq. (C21). In fact, this transfer matrix absorbs not $e^{-uN_{d0}}$, but instead $e^{-uN_{\pm0}/2}$ into itself. The factor $e^{-u\delta_{L_0,2N}}$ that also enters the definition of N_{d0} [see Eq. (C13)], is not absorbed into $\widetilde{T}$-matrix, because this term involves all the spins of the chain, which cannot be properly represented using a nearest neighbor transfer matrix formalism. As a consequence, we must keep in mind that the results of the sum over all configurations in Eq. (C19), will need to include an additional factor of e^{-u} in the cases where all the spins are unpolarized, i.e. when $L_0=2N$.

For domains of polarized spins, the sum over all configurations in Eq. (C20) is still computed using a modified transfer matrix. This $\widetilde{T}$-matrix is the same as that of Eq. (C21), defined for the case of unpolarized domains. However, if we remember the definition of the operator counting the number of polarized spins domains [see Eq. (C17)], $N_{d\pm}=N_{\pm0}/2+\delta_{L_\pm,2N}$, we readily conclude that now, our results will need to include an additional factor of e^{-u} in the cases where all the spins are polarized, i.e. $L_\pm=2N$, and not when $L_0=2N$.

Given this, we can rewrite the integrand in Eq. (C19) for the DSD of unpolarized spins, using the transfer matrix formalism as,

$$I_0(L) = \frac{1}{Z'_{2N}} \frac{\widetilde{Z}_{2N}}{L} \sum_{i=1}^{2N} \langle f^0_{i,L} \rangle_{\widetilde{T}} e^{-u\delta_{L,2N}}, \quad \text{(C22)}$$

where $\widetilde{Z}_{2N}$ is the partition function associated with the $\widetilde{T}$-matrix. In what concerns the computation of the DSD of $\pm$-spin domains, note that the integrand in Eq. (C20), $I_\pm(L)$, is of the same form as $I_0(L)$ on Eq. (C22), but with $f^0_{i,L}$ substituted by $f^\pm_{i,L}$,

$$I_\pm(L) = \frac{1}{Z'_{2N}} \frac{\widetilde{Z}_{2N}}{L} \sum_{i=1}^{2N} \langle f^\pm_{i,L} \rangle_{\widetilde{T}} e^{-u\delta_{L,2N}}, \quad \text{(C23)}$$

where we should recall that the Z'_{2N} in Eq. (C23) is different from that appearing in Eq. (C22). In addition, note that the exponential term in Eq. (C23) refers to the configuration where all the spins of the 1D chain are polarized, while such term in Eq. (C22) refers to the configuration where all the spins are unpolarized.

If we now define $\Theta(L)=\xi_i\xi_{i+1}\ldots\xi_{i+L-1}$ where $\xi_i\equiv 1-\sigma_i^2$, we can, using Eqs. (C3)-(C5), write Eq. (C22) as

$$\begin{aligned} I_0(L\leq 2N-2) &= 2N\frac{\widetilde{Z}_{2N}}{Z'_{2N}}\Big[\langle\Theta(L+2)\rangle_{\widetilde{T}} \\ &- 2\langle\Theta(L+1)\rangle_{\widetilde{T}}+\langle\Theta(L)\rangle_{\widetilde{T}}\Big] \quad \text{(C24a)} \\ I_0(L=2N-1) &= 2N\frac{\widetilde{Z}_{2N}}{Z'_{2N}}\Big[\langle\Theta(2N)\rangle_{\widetilde{T}} \\ &- \langle\Theta(2N-1)\rangle_{\widetilde{T}}\Big], \quad \text{(C24b)} \\ I_0(L=2N) &= \frac{\widetilde{Z}_{2N}}{Z'_{2N}}\langle\Theta(2N)\rangle_{\widetilde{T}}e^{-u}. \quad \text{(C24c)} \end{aligned}$$

In the case of the domains of polarized spins, in accordance with Eqs. (C6)-(C8), the integrands are obtained from Eqs. (C24), just by substituting $\Theta(L)$ by

$\Gamma(L) = \sigma_i^2\sigma_{i+1}^2\ldots\sigma_{i+L-1}^2$,

$$
\begin{aligned}
I_{\pm}(L\leq 2N-2) &= 2N\frac{\widetilde{Z}_{2N}}{Z'_{2N}}\Big[\langle\Gamma(L+2)\rangle_{\widetilde{T}} \\
&- 2\langle\Gamma(L+1)\rangle_{\widetilde{T}} + \langle\Gamma(L)\rangle_{\widetilde{T}}\Big], \quad \text{(C25a)}\\
I_{\pm}(L=2N-1) &= 2N\frac{\widetilde{Z}_{2N}}{Z'_{2N}}\Big[\langle\Gamma(2N)\rangle_{\widetilde{T}} \\
&- \langle\Gamma(2N-1)\rangle_{\widetilde{T}}\Big], \quad \text{(C25b)}\\
I_{\pm}(L=2N) &= \frac{\widetilde{Z}_{2N}}{Z'_{2N}}\langle\Gamma(2N)\rangle_{\widetilde{T}}e^{-u}. \quad \text{(C25c)}
\end{aligned}
$$

Computing the correlation functions $\langle\Theta(L)\rangle_{\widetilde{T}}$, using the transfer matrix formalism involves the computation of the following trace

$$
\langle\Theta(L)\rangle_{\widetilde{T}} = \frac{1}{\widetilde{Z}_{2N}}\mathrm{Tr}\Big[\widetilde{T}^{2N-L}(\xi\widetilde{T})^L\Big], \quad \text{(C26)}
$$

which yields the result $\langle\Theta(L)\rangle_{\widetilde{T}} = \widetilde{F}(1)^{L-1}\widetilde{F}(2N-L+1)/\big(\widetilde{Z}_{2N}\widetilde{F}(0)^L\big)$, where $\widetilde{F}(r) = \widetilde{\alpha}_+\widetilde{\beta}_-\widetilde{\lambda}_-^r - \widetilde{\alpha}_-\widetilde{\beta}_+\widetilde{\lambda}_+^r$. The $\widetilde{\alpha}_\pm$ and $\widetilde{\beta}_\pm$ are the entries of the eigenvectors of $\widetilde{T}$, $|\lambda_\pm\rangle$ [see Eq. (B5)]. Noting that $\widetilde{F}(1) = \widetilde{F}(0)$ and using Eq. (B5), we can finally write $\langle\Theta(L)\rangle_{\widetilde{T}}$ as

$$
\langle\Theta(L)\rangle_{\widetilde{T}} = \frac{1}{\widetilde{Z}_{2N}}\frac{(\widetilde{\lambda}_+-1)\widetilde{\lambda}_-^p - (\widetilde{\lambda}_--1)\widetilde{\lambda}_+^p}{\sqrt{(e^{-\beta\delta}-1)^2+8e^{-2\beta\widetilde{\gamma}}}}, \quad \text{(C27)}
$$

where $p = 2N-(L-1)$.

In the computation of the DSD of the polarized spins, the $\langle\Gamma(L)\rangle_{\widetilde{T}}$ appearing in Eqs. (C25) can be analogously computed and one obtains

$$
\begin{aligned}
\langle\Gamma(L)\rangle_{\widetilde{T}} &= \frac{e^{-\beta\delta(L-1)}}{\widetilde{Z}_{2N}}\frac{(\widetilde{\lambda}_+-1)\widetilde{\lambda}_+^p - (\widetilde{\lambda}_--1)\widetilde{\lambda}_-^p}{\sqrt{(e^{-\beta\delta}-1)^2+8e^{-2\beta\widetilde{\gamma}}}} \\
&+ \frac{\lambda_0^{2N}}{\widetilde{Z}_{2N}}, \quad \text{(C28)}
\end{aligned}
$$

where, again, $p = 2N-(L-1)$.

The integrands in Eqs. (C24) can be rewritten as

$$
\begin{aligned}
I_0(L\leq 2N-2) &= 2N\frac{1}{Z'_{2N}}\Big(W_- - W_+\Big), \quad \text{(C29a)}\\
I_0(L=2N-1) &= 2N\frac{1}{Z'_{2N}}\Big(Y_- - Y_+\Big), \quad \text{(C29b)}\\
I_0(L=2N) &= \frac{1}{Z'_{2N}}e^{-u}, \quad \text{(C29c)}
\end{aligned}
$$

where $W_\pm = \widetilde{\lambda}_\mp^{p-2}(\widetilde{\lambda}_\pm-1)(\widetilde{\lambda}_\mp-1)^2/(\widetilde{\lambda}_+-\widetilde{\lambda}_-)$, while $Y_\pm = \widetilde{\lambda}_\mp^{p-1}(\widetilde{\lambda}_\pm-1)(\widetilde{\lambda}_\mp-1)/(\widetilde{\lambda}_+-\widetilde{\lambda}_-)$.

For the polarized spins domains case, the integrands in Eqs. (C25) can be rewritten as

$$
\begin{aligned}
I_{\pm}(L\leq 2N-2) &= 2N\frac{1}{Z'_{2N}}\Big(\mathcal{W}_- - \mathcal{W}_+\Big), \quad \text{(C30a)}\\
I_{\pm}(L=2N-1) &= 2N\frac{1}{Z'_{2N}}\Big(\mathcal{Y}_- - \mathcal{Y}_+\Big), \quad \text{(C30b)}\\
I_{\pm}(L=2N) &= \frac{2\lambda_0^{2N}}{Z'_{2N}}e^{-u}, \quad \text{(C30c)}
\end{aligned}
$$

where $\mathcal{W}_\pm = e^{-\beta\delta(L-1)}\widetilde{\lambda}_\pm^{p-2}(\widetilde{\lambda}_\pm-1)(\widetilde{\lambda}_\pm-e^{-\beta\delta})^2/(\widetilde{\lambda}_+-\widetilde{\lambda}_-)$, while $\mathcal{Y}_\pm = e^{-\beta\delta(L-1)}\widetilde{\lambda}_\pm^{p-1}(\widetilde{\lambda}_\pm-1)(\widetilde{\lambda}_\pm-e^{-\beta\delta})/(\widetilde{\lambda}_+-\widetilde{\lambda}_-)$.

Performing the integral over u in the expressions for $I_0(L)$ as given in Eqs.(C29), leaves us with the following expressions for the DSD of unpolarized spins

$$
\begin{aligned}
\left\langle\frac{N_{d_L}^0}{N_{d0}}\right\rangle_{L\leq 2N-2} &= \frac{2N}{Z'_{2N}}\frac{1}{2^{m+2}}\Bigg[\frac{1}{m+1}\Big\{c\Big(G_-^{m+1}+G_+^{m+1}\Big) - \sqrt{c^2+d}\Big(G_-^{m+1}-G_+^{m+1}\Big) - 2c\Big(2(c+1)\Big)^{m+1}\Big\} \\
&- \frac{1}{(m+1)(m+2)}\Big\{\Big(G_-^{m+2}+G_+^{m+2}\Big) - 2^{m+2}\Big(1+(c+1)^{m+2}\Big)\Big\}\Bigg], \quad \text{(C31a)}\\
\left\langle\frac{N_{d_L}^0}{N_{d0}}\right\rangle_{L=2N-1} &= \frac{2N}{Z'_{2N}}\frac{1}{8}\Big[\Big(G_-^2+G_+^2\Big) - 4\Big(1+(c+1)^2\Big)\Big], \quad \text{(C31b)}\\
\left\langle\frac{N_{d_L}^0}{N_{d0}}\right\rangle_{L=2N} &= \frac{1}{Z'_{2N}}, \quad \text{(C31c)}
\end{aligned}
$$

with $m = p-2$, $G_\pm = c+2\pm\sqrt{c^2+d}$, $c = e^{-\beta\delta}-1$ and $d = 8e^{-\beta\gamma}$. Recall that, as the above equations refer to

the computation of the DSD of 0-spins, in Eqs. (C31) we have that $Z'_{2N} = \lambda_+^{2N} - \lambda_0^{2N} + \lambda_-^{2N}$.

The DSD of polarized spins, is analogously given from Eqs.(C30), by

$$\left\langle \frac{N^{\pm}_{d_L}}{N_{d\pm}} \right\rangle_{L\leq 2N-2} = \frac{2N}{Z'_{2N}} \frac{e^{-\beta\delta(L-1)}}{2^{m+2}} \left[\frac{1}{m+1} \left\{ \bar{c}\left(\mathcal{G}_-^{m+1} + \mathcal{G}_+^{m+1}\right) - \sqrt{\bar{c}^2+d}\left(\mathcal{G}_-^{m+1} - \mathcal{G}_+^{m+1}\right) - 2^{2m+2}\bar{c} \right\} \right.$$
$$\left. - \frac{1}{(m+1)(m+2)} \left\{ \left(\mathcal{G}_-^{m+2} + \mathcal{G}_+^{m+2}\right) - 2^{m+2}\left(1 + (1-\bar{c})^{m+2}\right) \right\} \right], \tag{C32a}$$

$$\left\langle \frac{N^{\pm}_{d_L}}{N_{d\pm}} \right\rangle_{L=2N-1} = \frac{2N}{Z'_{2N}} \frac{e^{-\beta\delta(2N-2)}}{8} \left[\left(G_-^2 + G_+^2\right) - 4\left(1 + (1-\bar{c})^2\right) \right], \tag{C32b}$$

$$\left\langle \frac{N^{\pm}_{d_L}}{N_{d\pm}} \right\rangle_{L=2N} = \frac{2\lambda_0^{2N}}{Z'_{2N}}, \tag{C32c}$$

with $\bar{c} = 1 - e^{-\beta\delta}$ and $\mathcal{G}_\pm = 2 - \bar{c} \pm \sqrt{\bar{c}^2 + d}$. As Eqs. (C32) refer to the DSD of $\pm$-spins, the Z'_{2N} appearing in Eqs. (C32) reads $Z'_{2N} = \lambda_+^{2N} + \lambda_0^{2N} + \lambda_-^{2N} - 1$.

b. *The thermodynamic limit of the DSD*

In the thermodynamic limit ($2N \to \infty$), when the domain size is much smaller than the size of the system ($L \ll 2N$), we can perform the limit $m \to +\infty$ in Eq. (C31a). Note that as $G_+ > G_-$, $c+1 > 1$ and $G_+ > 2(c+1)$, then we have that the DSD of unpolarized spins, in the thermodynamic limit, is given by Eq. (12). Analogously, the DSD of polarized spins, also in the thermodynamic limit, is given by Eq. (11).

In Fig. 11, we have plotted the DSD of unpolarized spins at a non-passivated edge, as well as the DSD of polarized spins at a hydrogen-passivated one, for two sets of particular values of the exchange parameters. In these plots we have used, the values for the exchange parameters γ and δ computed in Appendix A, i.e. $\gamma = 0.03$ and $\delta = -0.49$ for the unpassivated edge and $\gamma = 0.52$ and $\delta = 0.66$ for the hydrogen-passivated edge. We readily see that both DSDs strongly decrease with increasing sizes of the domains. Note the dependence of such decrease rate with the temperature: the larger the temperature is, the smaller the decrease rate is.

A distribution $P(x)$ is said to have fat tails if it displays a slower decrease than the normal distribution, (or, alternatively, if it decreases with a power of x) when $x \to \infty$. As a consequence, the moments of a fat-tailed distribution diverge above a given order, characteristic of that distribution, and thus its characteristic function is not analytical at the origin.

Let us now consider the question of whether the DSDs computed above display fat tails in the thermodynamic limit (let us represent the DSD generically as $\mathcal{P}(L)$). Its characteristic function is given by the discrete Fourier transform

$$\hat{\mathcal{P}}(w) = \sum_{n=1}^{+\infty} e^{iwn} \mathcal{P}(L). \tag{C33}$$

The characteristic functions of $\mathcal{P}_0(L)$ and of $\mathcal{P}_\pm(L)$ are geometric series, and hence easily computable, after which we obtain Eq. (14) and Eq. (13).

From Eq. (14), or its geometric series form, we con-

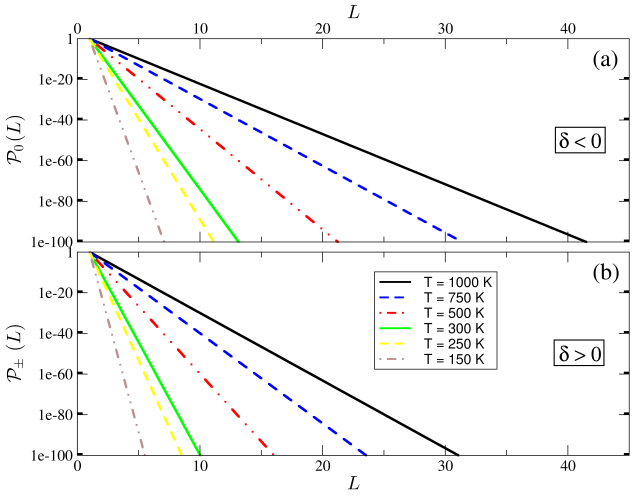

FIG. 11: (Color online) Plots of the DSD for two sets of values of the exchange parameters γ and δ. In both panels we present the DSD (with a logarithmic scale in the y-axis) for six different temperatures: full black lines stand for $T = 1000K$; dashed blue lines stand for $T = 750K$; dash-dotted red lines stand for $T = 500K$; full light green lines stand for $T = 300K$; dashed light yellow lines stand for $T = 250K$; dash-dotted light brown lines stand for $T = 150K$. (a) DSD of unpolarized spins, in an unpassivated edge ($\gamma = 0.03$ and $\delta = -0.49$). (b) DSD of polarized spins, in a hydrogen-passivated edge ($\gamma = 0.52$ and $\delta = 0.66$).

clude that all the derivatives of $\hat{\mathcal{P}}_0(w)$ exist at $w = 0$, if $\lambda_+ > 1$. If the unpolarized spins are the minority spins in the chain, $\delta < 0$ and we have $\lambda_+ \geq 1 + \sqrt{2} > 1$ for every $\beta \geq 0$, thus $\mathcal{P}_0(L)$ has no fat-tails.

Similarly, from Eq. (13), when the polarized spins are the minority spins in the spin chain, $\delta > 0$ and we conclude that all the derivatives of $\hat{\mathcal{P}}_\pm(w)$ exist at $w = 0$, if $\lambda_+ e^{\beta\delta} > 1$. This is verified for every $\beta \geq 0$, since $\lambda_+ e^{\beta\delta} \geq 1 + \sqrt{2} > 1$. Again, we conclude that $\mathcal{P}_\pm(L)$ has no fat-tails.

The first moment of $\mathcal{P}_0(L)$ gives us the mean size of the domains of unpolarized spins in the thermodynamic limit, $\bar{L}_0$, which reads

$$\bar{L}_0 \;=\; -i\frac{\mathrm{d}}{\mathrm{d}w}\hat{\mathcal{P}}_0(w)\bigg|_{w=0}. \qquad \text{(C34)}$$

In the same way, we can compute the mean size of the domains of polarized spins (in the thermodynamic limit), $\bar{L}_\pm$. Both these two quantities are written, respectively, in Eqs. (16) and (15). These two quantities are plotted in Fig. 8.

* Electronic address: joaonbrod@gmail.com

1 K. S. Novoselov, A. K. Geim, S. V. Morozov, D. Jiang, Y. Zhang, S. V. Dubonos, I. V. Grigorieva, and A. A. Firsov, Science **306**, 666 (2004).

2 K. S. Novoselov, D. Jiang, F. Schedin, T. J. Booth, V. V. Khotkevich, S. V. Morozov, and A. K. Geim, PNAS **102**, 10451 (2005).

3 K. S. Novoselov, A. K. Geim, S. V. Morozov, D. Jiang, M. I. Katsnelson, I. V. Grigorieva, S. V. Dubonos, and A. A. Firsov, Nature **438**, 197 (2005).

4 Y. B. Zhang, Y. W. Tan, H. L. Stormer, and P. Kim, Nature **438**, 201 (2005).

5 A. H. Castro Neto, F. Guinea, N. M. R. Peres, K. S. Novoselov, and A. K. Geim, Rev. Mod. Phys. **81**, 109 (2009).

6 N. M. R. Peres, Rev. Mod. Phys. **82**, 2673 (2010).

7 X. J. and, Nanoscale **3**, 86 (2011).

8 F. Molitor, J. Güttinger, C. Stampfer, S. Dröscher, A. Jacobsen, T. Ihn, and K. Ensslin, J. Phys.: Condens. Matter **23**, 243201 (2011).

9 S. D. Sarma, S. Adam, E. Hwang, and E. Rossi, Rev. Mod. Phys. **83**, 407 (2011).

10 R. P. Wallace, Phys. Rev. **71**, 329 (1947).

11 X. Wang, L. J. Zhi, and K. Mullen, Nano Lett. **8**, 323 (2008).

12 P. Blake, P. D. Brimicombe, R. R. Nair, T. J. Booth, D. Jiang, F. Schedin, L. A. Ponomarenko, S. V. Morozov, H. F. Gleeson, E. W. Hill, et al., Nano Lett. **8**, 1704 (2008).

13 F. Schedin, A. K. Geim, S. V. Morozov, E. W. Hill, P. Blake, M. I. Katsnelson, and K. S. Novoselov, Nature Materials **6**, 652 (2007).

14 X. R. Wang, Y. J. Ouyang, X. L. Li, H. L. Wang, J. Guo, and H. J. Dai, Phys. Rev. Lett. **100**, 206803 (2008).

15 M. Fujita, K. Wakabayashi, K. Nakada, and K. Kusakabe, J. Phys. Soc. Jpn. **65**, 1920 (1996).

16 K. Nakada, M. Fujita, G. Dresselhaus, and M. S. Dresselhaus, Phys. Rev. B **54**, 17954 (1996).

17 K. Wakabayashi, M. Fujita, H. Ajiki, and M. Sigrist, Phys. Rev. B **59**, 8271 (1999).

18 V. Barone, O. Hod, and G. E. Scuseria, Nano Lett. **6**, 2748 (2006).

19 Y. Son, M. Cohen, and S. Louie, Nature **444**, 347 (2006).

20 C. H. Lewenkopf, E. R. Mucciolo, and A. H. Castro Neto, Phys. Rev. B **77**, 081410 (2008), URL `http://link.aps.org/doi/10.1103/PhysRevB.77.081410`.

21 E. R. Mucciolo, A. H. Castro Neto, and C. H. Lewenkopf, Phys. Rev. B **79**, 075407 (2009), URL `http://link.aps.org/doi/10.1103/PhysRevB.79.075407`.

22 V. M. Pereira, F. Guinea, J. M. B. Lopes dos Santos, N. M. R. Peres, and A. H. Castro Neto, Phys. Rev. Lett. **96**, 036801 (2006), URL `http://link.aps.org/doi/10.1103/PhysRevLett.96.036801`.

23 F. Sols, F. Guinea, and A. H. C. Neto, Phys. Rev. Lett. **99**, 166803 (2007).

24 M. Y. Han, B. Özyilmaz, Y. Zhang, and P. Kim, Phys. Rev. Lett. **98**, 206805 (2007), URL `http://link.aps.org/doi/10.1103/PhysRevLett.98.206805`.

25 L. A. Ponomarenko, F. Schedin, M. I. Katsnelson, R. Yang, E. W. Hill, K. S. Novoselov, and A. K. Geim, Science **320**, 356 (2008), http://www.sciencemag.org/content/320/5874/356.full.pdf, URL `http://www.sciencemag.org/content/320/5874/356.abstract`.

26 M. Y. Han, J. C. Brant, and P. Kim, Phys. Rev. Lett. **104**, 056801 (2010), URL `http://link.aps.org/doi/10.1103/PhysRevLett.104.056801`.

27 L. Xie, H. Wang, C. Jin, X. Wang, L. Jiao, K. Suenaga, and H. Dai, Journal of the American Chemical Society **133**, 10394 (2011), http://pubs.acs.org/doi/pdf/10.1021/ja203860a, URL `http://pubs.acs.org/doi/abs/10.1021/ja203860a`.

28 A. Stone and D. Wales, Chem. Phys. Lett. **128**, 501 (1986).

29 J. Meyer, C. Kisielowski, R. Emi, M. Rossell, M. Crommie, and A. Zettl, Nano Lett. **8**, 3582 (2008).

30 K. Zakharchenko, A. Fasolino, J. Los, and M. Katsnelson, J. Phys.: Condens. Matter **23**, 202202 (2011).

31 R. Y. Oeiras, F. M. Araujo-Moreira, and E. Z. da Silva, Phys. Rev. B **80**, 073405 (2009).

32 P. Koskinen, S. Malola, and H. Hakkinen, Phys. Rev. Lett. **101**, 115502 (2008).

33 B. Huang, M. Liu, N. Su, J. Wu, W. Duan, B. Gu, , and F. Liu, Phys. Rev. Lett. **102**, 166404 (2009).

34 S. Bhowmick and U. Waghmare, Phys. Rev. B **81**, 155416 (2010).

35 J. N. B. Rodrigues, P. A. D. Gonçalves, N. F. G. Rodrigues, R. M. Ribeiro, J. M. B. Lopes dos Santos, and N. M. R. Peres, Phys. Rev. B **84**, 155435 (2011), URL `http://link.aps.org/doi/10.1103/PhysRevB.84.155435`.

36 J. A. M. van Ostaay, A. R. Akhmerov, C. W. J. Beenakker, and M. Wimmer, Phys. Rev. B **84**, 195434 (2011), URL `http://link.aps.org/doi/10.1103/PhysRevB.84.195434`.

37 G. Lee, C. Wang, E. Yoon, N. Hwang, and K. Ho, Phys.

Rev. B **81**, 195419 (2010).
[38] J. Li, Z. Li, G. Zhou, Z. Liu, J. Wu, B.-L. Gu, J. Ihm, and W. Duan, Phys. Rev. B **82**, 115410 (2010), URL `http://link.aps.org/doi/10.1103/PhysRevB.82.115410`.
[39] J. Kroes, M. Akhukov, J. Los, N. Pineau, and A. Fasolino, Phys. Rev. B **83**, 165411 (2011).
[40] T. Wassmann, A. Seitsonen, A. Saitta, M. Lazzeri, and F. Mauri, Phys. Rev. Lett. **101**, 096402 (2008).
[41] C. Girit, J. Meyer, R. Erni, M. Rossell, C. Kisielowski, L. Yang, C. Park, M. Crommie, M. Cohen, S. Louie, et al., Science **323**, 1705 (2009).
[42] A. Chuvilin, J. Meyer, G. Algara-Siller, and U. Kaiser, New J. Phys. **11**, 083019 (2009).
[43] P. Koskinen, S. Malola, and H. Hakkinen, Phys. Rev. B **80**, 073401 (2009).
[44] K. Suenaga and M. Koshino, Nature **468**, 1088 (2010).
[45] J. Warner, E. Margine, M. Mukai, A. Robertson, F. Giustino, and A. Kirkland, Science **337**, 209 (2012).
[46] S. Malola, H. Hakkinen, and P. Koskinen, Eur. Phys. J. D **52**, 71 (2009).
[47] P. Rakyta, A. Kormányos, J. Cserti, and P. Koskinen, Phys. Rev. B **81**, 115411 (2010).
[48] K. Huang, Statistical Mechanics (John Wiley, 1987), 2nd ed.
[49] F. Rys, Helv. Phys. Acta **42**, 606 (1969).
[50] A. Hintermann and F. Rys, Helv. Phys. Acta **42**, 608 (1969).
[51] M. Blume, V. J. Emery, and R. B. Griffiths, Phys. Rev. A **4**, 1071 (1971), URL `http://link.aps.org/doi/10.1103/PhysRevA.4.1071`.
[52] M. J. Rayson and P. R. Briddon, Comput. Phys. Commun. **178**, 128 (2008).
[53] H. J. Monkhorst and J. D. Pack, Phys. Rev. B **13**, 5188 (1976).
[54] C. Hartwigsen, S. Goedecker, and J. Hutter., Phys. Rev. B **58**, 3641 (1998).